Article

Cell

GPR68 Senses Flow and Is Essential for Vascular Physiology

Graphical Abstract

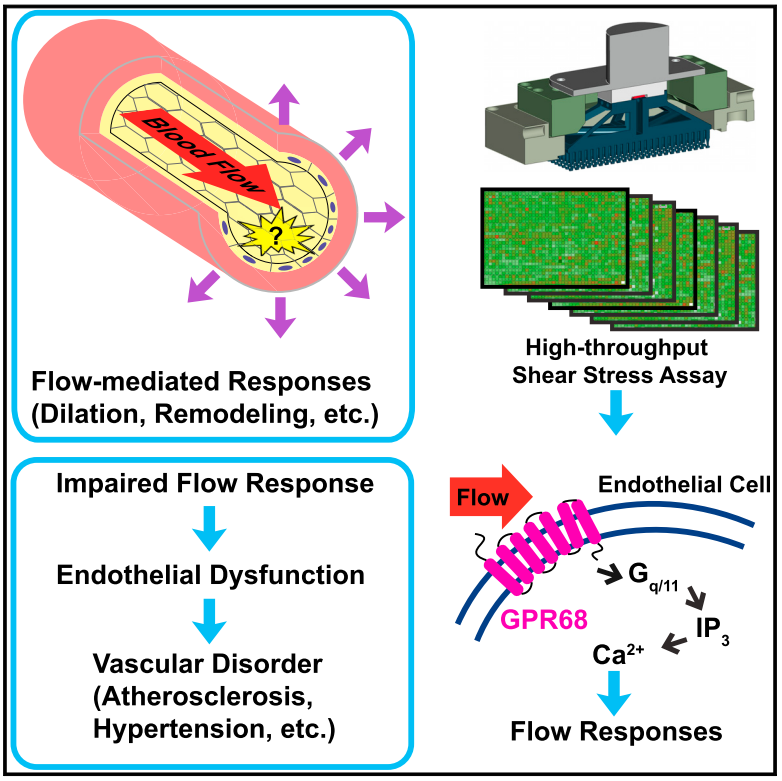

Authors

Jie Xu, Jayanti Mathur, Emilie Vessières, ..., Shu Chien, Daniel Henrion, Ardem Patapoutian

Correspondence

ardem@scripps.edu

In Brief

A GPCR is a critical sensor for fluid shear stress in blood vessels.

Highlights

- Design of a novel high-throughput assay for cellular mechanosensation
- An RNAi screen identifies GPR68 as a mechanosensor
- GPR68 is necessary and sufficient for responses to fluid shear stress
- GPR68 is required for flow-induced dilation and remodeling in mice

Xu et al., 2018, Cell *173*, 762–775
April 19, 2018 © 2018 Elsevier Inc.
https://doi.org/10.1016/j.cell.2018.03.076

CellPress

Cell

Article

GPR68 Senses Flow and Is Essential for Vascular Physiology

Jie Xu,[1] Jayanti Mathur,[1] Emilie Vessières,[2] Scott Hammack,[1] Keiko Nonomura,[3,6] Julie Favre,[2] Linda Grimaud,[2] Matt Petrus,[1] Allain Francisco,[3] Jingyuan Li,[1] Van Lee,[1] Fu-li Xiang,[1] James K. Mainquist,[1] Stuart M. Cahalan,[3,7] Anthony P. Orth,[1] John R. Walker,[1] Shang Ma,[3] Viktor Lukacs,[3] Laura Bordone,[1] Michael Bandell,[1] Bryan Laffitte,[1] Yan Xu,[4] Shu Chien,[5] Daniel Henrion,[2] and Ardem Patapoutian[3,8,*]

[1]Genomics Institute of the Novartis Research Foundation, San Diego, CA 92121, USA
[2]MITOVASC Institute, CARFI Facility, CNRS UMR 6015, INSERM U1083, Angers University, Angers, France
[3]Doris Neuroscience Center, Howard Hughes Medical Institute, the Scripps Research Institute, La Jolla, CA 92037, USA
[4]Department of Obstetrics and Gynecology, Indiana University School of Medicine, Indianapolis, IN 46202, USA
[5]Departments of Bioengineering and Medicine, and Institute of Engineering in Medicine, University of California, San Diego, La Jolla, CA 92093, USA
[6]Present address: National Institute for Basic Biology, Division of Embryology, 5-1 Higashiyama, Myodaiji, Okazaki, Aichi 444-8787, Japan
[7]Present address: Vertex Pharmaceuticals, 11010 Torreyana Road, San Diego, CA 92121, USA
[8]Lead Contact
*Correspondence: ardem@scripps.edu
https://doi.org/10.1016/j.cell.2018.03.076

SUMMARY

Mechanotransduction plays a crucial role in vascular biology. One example of this is the local regulation of vascular resistance via flow-mediated dilation (FMD). Impairment of this process is a hallmark of endothelial dysfunction and a precursor to a wide array of vascular diseases, such as hypertension and atherosclerosis. Yet the molecules responsible for sensing flow (shear stress) within endothelial cells remain largely unknown. We designed a 384-well screening system that applies shear stress on cultured cells. We identified a mechanosensitive cell line that exhibits shear stress-activated calcium transients, screened a focused RNAi library, and identified GPR68 as necessary and sufficient for shear stress responses. GPR68 is expressed in endothelial cells of small-diameter (resistance) arteries. Importantly, Gpr68-deficient mice display markedly impaired acute FMD and chronic flow-mediated outward remodeling in mesenteric arterioles. Therefore, GPR68 is an essential flow sensor in arteriolar endothelium and is a critical signaling component in cardiovascular pathophysiology.

INTRODUCTION

Mechanotransduction is the central feature of many biological processes, including the sensing of touch and pain, hearing, cardiovascular dynamics, and turgor pressure sensing in bacteria. Several membrane proteins capable of sensing acute mechanical forces have been identified, including the ion channels MscL and MscS in bacteria, the degenerin/epithelial Na^+ channel (DEG/ENaC) MEC-4/MEC-10 and transient receptor potential (TRP) channel TRP-4 in *C. elegans*, and no mechanoreceptor potential C (NOMPC) in *Drosophila* (Driscoll and Chalfie, 1991; Huang and Chalfie, 1994; Kang et al., 2010; Levina et al., 1999; Li et al., 2006; Sukharev et al., 1994; Walker et al., 2000; Yan et al., 2013).

In vertebrates, the identity of mechanosensors has been more elusive. First identified in mammals, Piezos are a family of mechanically activated ion channels conserved through evolution (Coste et al., 2010). Piezos play crucial roles in various physiological settings, e.g., somatosensation, vascular development, and function (Li et al., 2014; Lukacs et al., 2015; Nonomura et al., 2017; Ranade et al., 2014; Retailleau et al., 2015; Wang et al., 2016; Woo et al., 2014). Within the vascular system, Piezo1 in smooth muscle cells plays a role in hypertension-dependent arterial remodeling (Retailleau et al., 2015). In endothelial cells, Piezo1- deficiency causes compromised flow-mediated vasodilation and increased systolic blood pressure (Wang et al., 2016). However, another report did not find evidence for hypertension in Piezo1-deficient mice and showed a requirement of Piezo1 in flow-mediated vasoconstriction instead (Rode et al., 2017). Regardless of the precise role of Piezo1, an understanding of how blood vessels sense shear stress or pressure is in its infancy.

Beyond ion channels, G protein-coupled receptors (GPCRs) are sensory molecules responsible for vision, smell, and taste, among other functions. In addition, a number of GPCRs, including angiotensin II receptor type 1 (AGTR1), bradykinin receptor B2 (BDKRB2), and parathyroid hormone 1 receptor (PTH1R), have been proposed as mechanosensors in various physiological settings, including cardiovascular physiology (Chachisvilis et al., 2006; Mederos y Schnitzler et al., 2008; Zhang et al., 2009). However, evidence that these GPCRs are both necessary and sufficient for acute mechanotransduction in an *in vivo* setting is lacking. Regardless, there is evidence that GPCR signaling is important for mechanotransduction in vasculature. For example, acute shear stress imposed by blood flow on vessel endothelial cells induces diverse downstream

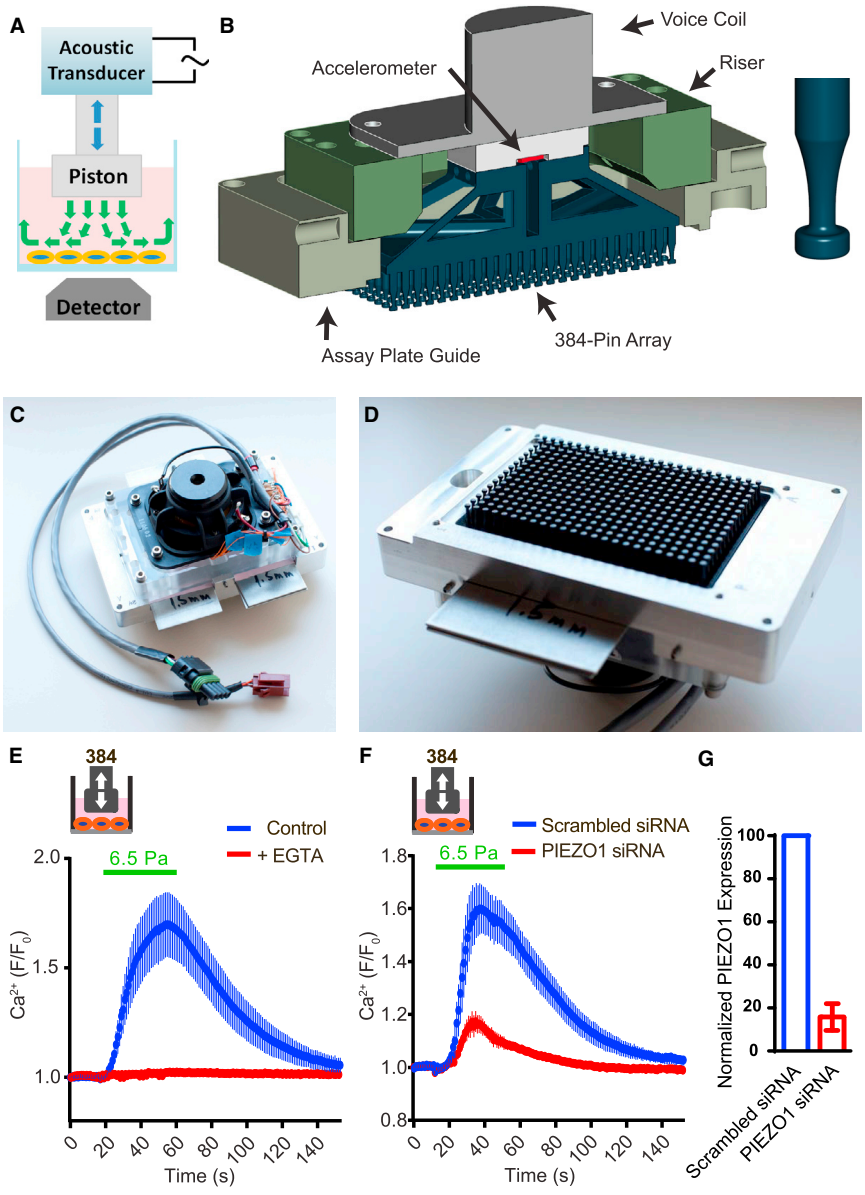

Figure 1. Construction and Validation of 384-Well High-Throughput Shear Stress Stimulation System

(A) Schematic representation of the disturbed flow stimulation system.

(B) Left: drawing depicts the major components. Right: the bubble-relief geometry of the stimulator pins.

(C) Top view showing the acoustic transducer assembly.

(D) Bottom view showing the 384-pin array.

(E) Intracellular calcium levels of HeLa cells measured by FLIPR under 6.5 Pa shear stress stimulation in the presence of 2.5 mM EGTA or untreated control. The viscosity of the assay buffer was increased to 8.37×10^{-3} Pa·s by adding PVP to 2% (w/w). Disturbed flow (0.2 s on, 2 s off) was applied at 60 Hz for 40 s. Data are the average of 48 wells from 3 trials for each condition.

(F) Intracellular calcium levels of HUVECs under the same disturbed flow stimulation after the treatment of scrambled siRNA or hPIEZO1 siRNA. Data are the average of 48 wells from 3 trials for each condition.

(G) Relative mRNA level of PIEZO1 in HUVECs transfected with PIEZO1 siRNA compared with cells treated with scrambled siRNA (n = 3).

See also Figure S1.

signaling events, most notably the phospholipase C (PLC)-dependent increase in intracellular calcium concentrations mainly via unknown mechanisms (Ishida et al., 1997; Melchior and Frangos, 2012). However, the identity of the putative mechanosensitive GPCRs *in vivo* remains unknown.

Finally, beyond hearing, somatosensation, and vascular biology, many other cell types within bone, muscle, lung, kidney, eye, and other tissues respond to mechanical stimuli through unknown mechanisms (Jaalouk and Lammerding, 2009). We previously conducted a functional genomic small interfering RNA (siRNA) screen to identify Piezo1 using membrane indentation and electrophysiological recording (Coste et al., 2010). It was a low-throughput screen that required a year to identify Piezo1 after screening 71 other candidate genes. Here, we aimed to accelerate genomic screens relevant to mechanotransduction by designing a novel high-throughput (HT) mechanical stimulation system. Using this novel assay, we identified a bona fide shear stress sensor GPR68 and show that it plays a crucial role in vascular physiology and pathophysiology. These findings demonstrate that GPCRs, as well as ion channels, can function as *in vivo* shear stress sensors.

RESULTS

A Novel 384-Well Mechanical Stimulation Assay

Among different types of mechanical forces, fluid shear stress is perhaps the most amenable to an HT assay format, and physiologically relevant flow sensors in vascular biology are mainly unknown. Our design concept featured a flat-headed piston driven by an acoustic transducer controlled by a signal generator (Figure 1A). During operation, the piston was immersed in buffer in a transparent-bottom welled plate, moving up and down at commanded frequency and amplitude to create disturbed fluid motion with an oscillatory fashion. The moving fluid imposes shear stress on the cells cultured at the bottom of the chamber. The response of the cells can be imaged by a detector below the plate (Figure 1A). After validation, we scaled up the system to 384-well format by 3D printing a 384-pin stimulation array and then affixed it to a voice coil (Figure 1B). We optimized the shape of the pins to avoid trapping air bubbles in the plate (Figure 1B [right]). The

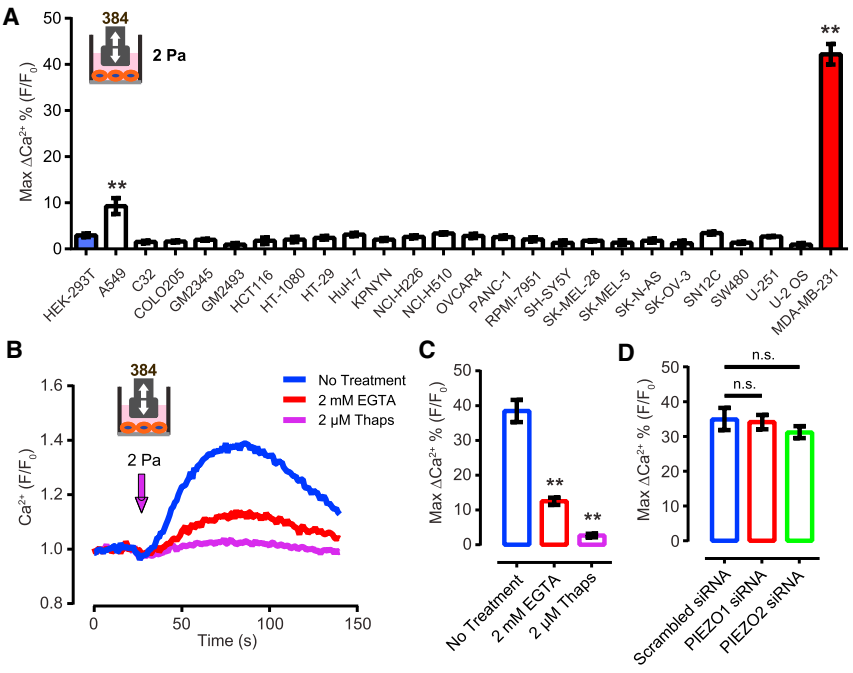

Figure 2. MDA-MB-231 Cells Show PIEZO1- and PIEZO2-Independent Shear Stress-Induced Calcium Transients

(A) Responses of various human cancer cell lines to shear stress at 2 Pa, 60 Hz with 0.2 s on, 2 s off for 40 s. **$p < 0.01$.

(B) The response of MDA-MB-231 cells to shear stress at 2 Pa, measured by FLIPR. The shear stress was applied for 4 s at 60 Hz. EGTA was added to the cells 2 min prior to the onset of shear stress. Thapsigargin was incubated with cells for 15 min before the shear stress stimulation.

(C) Quantification of the MDA-MB-231 cells' response to shear stress in the presence of EGTA and thapsigargin. **$p < 0.01$.

(D) Quantification of the MDA-MB-231 cells' response to shear stress 72 hr after transfection of PIEZO1 and PIEZO2 siRNA. n.s., not significant.

system fits inside the Molecular Devices fluorescence image plate reader (FLIPR Tetra) (Figures 1C and 1D). We measured the intensity of the shear stress generated by the HT system using particle image velocimetry and found that it is between 0.1–2 Pa (Ranade et al., 2014). We can increase the intensity of the shear stress up to ~16.7 Pa by increasing the viscosity of the buffer using polyvinylpyrrolidone (PVP), a bio-compatible, water-soluble polymer.

Next, we asked if human umbilical vein endothelial cells (HUVECs) could be acutely activated by the HT system using intracellular calcium level as a readout. HUVECs express endogenous PIEZO1 and show PIEZO1-dependent alignment to the direction of flow (Li et al., 2014; Ranade et al., 2014). Indeed, we observed robust transient increase in intracellular calcium levels in HUVECs when stimulated with shear stress at 6.5 Pa and above (with increased viscosity by PVP) (Figure 1E). The shear stress-induced calcium transients were completely abolished by 2.5 mM EGTA, suggesting that the signal was caused by extracellular calcium entering the cells (Figure 1E). The response was greatly attenuated in cells treated with PIEZO1 siRNA (Figures 1F and 1G). These results demonstrate that our HT mechanical stimulation system is capable of applying physiologically relevant shear stress in a precise, quantitative, and reproducible fashion.

MDA-MB-231 Breast Cancer Cells Express an Unknown Shear Stress Sensor

We set three criteria for a cell line suitable for the HT siRNA screen of novel mechanosensitive receptors: (1) it must respond to our HT flow system by displaying calcium transients, (2) it must be transfectable by siRNA with satisfactory knockdown efficiency, and (3) the response to shear stress should not depend on PIEZO1 or PIEZO2. We compiled a list of candidate cell lines based on the National Cancer Institute 60 human tumor cell line collection (NCI-60), as cancer cell lines often misexpress various genes. We selected cell lines that have low levels of RNA transcripts of PIEZO1 and PIEZO2 with the data from http://biogps.org/#goto=welcome. Out of the 25 cell lines tested, the lung cancer cell line A549 and the breast cancer cell line MDA-MB-231 showed shear stress-evoked calcium transients (Figure 2A). MDA-MB-231 responded to disturbed shear stress of 2 Pa with robust signals, while those of A549 were relatively modest (Figure 2A). The signal in MDA-MB-231 cells was mostly abolished when the calcium stores of the cells were depleted by thapsigargin. Removing extracellular Ca^{2+} by incubating the cells with EGTA prior to the onset of shear stress greatly reduced, but did not abolish, the response (Figures 2B and 2C). This suggests that the calcium transients are store dependent and also partly depend on the entry of calcium from the intracellular space. Transfecting MDA-MB-231 cells with siRNA against PIEZO1 or PIEZO2 achieved 86% and 78% knockdown at the transcript level, respectively (Figure S1), and did not affect the shear stress response of MDA-MB-231 cells, suggesting an unknown molecule is responsible for sensing shear stress (Figure 2D).

GPR68 Is Required for Shear Stress Responses in MDA-MB-231 Cells

We focused on membrane-integrated proteins as the most probable candidates for novel mechanosensors. We constructed a library of siRNAs against genes encoding proteins with two or more predicted transmembrane domains (2+TM), a characteristic trait shared by ion channels and GPCRs. The library contains 21,925 unique siRNAs, targeting 3,175 unique reference sequences encoded by 2,765 unique genes, arranged in a singlet configuration—i.e., each well of the 384-well plate contains one siRNA oligo. On average, each gene is represented by eight siRNAs across the library, most of them located on different plates. We transfected the MDA-MB-231 cells with the siRNA library and carried out the screen using the HT shear stress

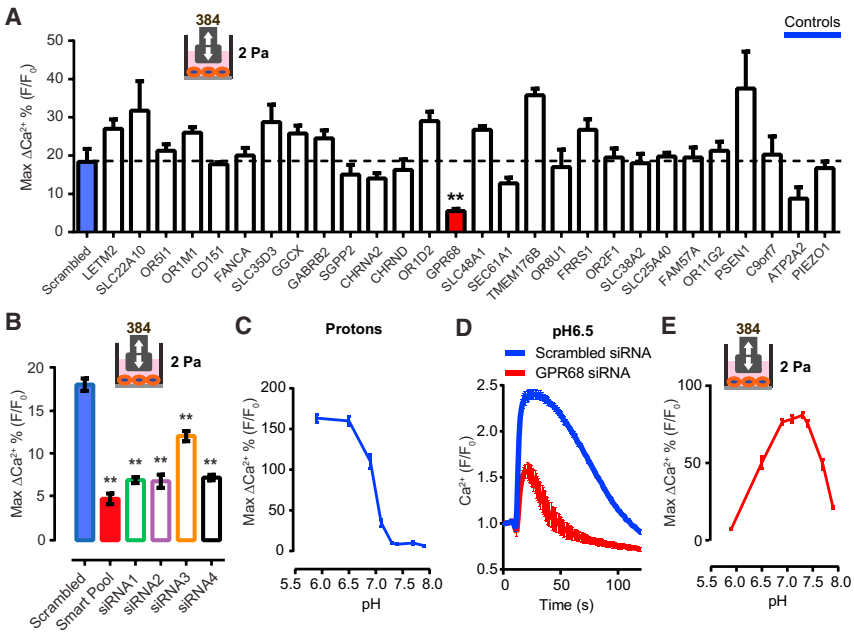

Figure 3. GPR68 Is Necessary for Shear Stress-Induced Calcium Transients in MDA-MB-231 Cells

(A) The response of MDA-MB-231 cells after treatment of siRNAs against the indicated candidates. **$p < 0.01$.

(B) Quantification of the MDA-MB-231 cells' response to shear stress after treatment with Smart Pool siRNA oligos and the individual siRNA oligos against GPR68. **$p < 0.01$.

(C) Response of MDA-MB-231 cells to proton stimulation at various final pH. The cells were incubated with Hank's balanced salt solution (HBSS) at pH 7.4 before the addition of the HBSS with various acidity. n = 3.

(D) The response of MDA-MB-231 cells to proton stimulation (final pH 6.5) after knocking down GPR68 by siRNA SMARTpool.

(E) The response of MDA-MB-231 cells to shear stress stimulation in buffers with various pH. The cells were incubated with assay buffer at pH 7.4. The pH was then changed by adding buffer with various acidity 3 min prior to the onset of shear stress stimulation.

See also Figure S2.

system. The primary screen yielded 56 hits, of which 26 were reconfirmed in a secondary screen. Of the 26 genes, GPR68 was the only one in the final confirmation run to show significantly reduced calcium transients caused by disturbed shear stress upon knockdown (Figure 3A). siRNAs targeting different regions of GPR68 were all effective in inhibiting the signal, suggesting that attenuation is not likely due to off-target effects (Figure 3B).

GPR68 was described to be a proton-activated GPCR. It is fully activated at pH 6.8 and is mostly inactive at pH 7.8 (Ludwig et al., 2003). Indeed, MDA-MB-231 cells showed little increase in intracellular calcium to pH 7.4 and above, while the response was maximal to stimulation by pH 6.5 and below (Figure 3C). Knocking down GPR68 significantly reduced proton-induced response (Figure 3D). We next tested shear stress response of MDA-MB-231 cells at various pH levels. We observed a bell-shaped curve such that shear stress is most effective at pH levels of 7.4–6.9 (normal arterial blood pH is ~7.4, and pH 6.9 represents severe acidosis) (Figure 3E) (Schwaderer and Schwartz, 2004). This suggests that GPR68 requires the presence of protons to sense shear stress. It was suggested that protonation leads to loss of bonding and repulsion between extracellular histidines, allowing the receptor to adopt an active conformation at physiological pH (Ludwig et al., 2003). We therefore tested a mutant of GPR68 where histidines 17, 20, 84, 169, and 269 were changed to phenylalanine and found that it lost both pH sensitivity and shear stress sensitivity (Figure S2A), supporting the notion that appropriate levels of proton must be present for the receptor to be activated. Hence, all follow-up experiments were carried out at pH 7.4.

GPR68 Is Activated by Shear Stress Imposed by Disturbed and Laminar Flow

To test if GPR68 activation is sufficient to confer mechanosensitivity, we transiently transfected GPR68 in human embryonic kidney (HEK) 293T cells and applied shear stress. HEK cells expressing human GPR68 showed an increase in intracellular calcium levels in response to 2 Pa shear stress, while vector-transfected cells were not responsive (Figure 4A). The amplitude of the calcium signals was dependent on the intensity of shear stress applied (Figure 4B). The maximum amplitude of the shear stress response is ~70% of the response when stimulated with extracellular proton at pH 6.5 (Figure 4C), implying that shear stress responses are overall comparable to the acid responses. The slightly lower response may be due to the fact that not all GPR68 proteins on the cell membrane experience shear stress as they would experience changes in pH. Notably, the responses were completely abolished by U73122, a PLC inhibitor, suggesting that the signal is indeed dependent on the activity of GPR68, a $G_{q/11}$-coupled receptor (Figure 4D). Proton-induced GPR68 activity is acutely blocked by Cu^{2+} (Ludwig et al., 2003), and 20 μM Cu^{2+} also blocked the shear stress-induced calcium signal (Figure 4D). This acute blockage of shear stress response argues against the possibility that overexpression of GPR68 causes alterations HEK cells that indirectly induce mechanosensitivity. One possible mechanism is that shear stress causes a decrease in pH, which in turn activates GPR68 indirectly. We measured both extracellular and intracellular pH real time by fluorescence imaging and found no change in either upon the application of shear stress (Figures S2B–S2D). Together, our data provide evidence for a necessary and sufficient role of GPR68 in the shear stress-induced release of calcium from stores.

Many GPCRs have been proposed to be mechanosensitive, although direct activation by mechanical forces (on the order of seconds) has not been demonstrated using intracellular calcium as a readout (Storch et al., 2012). To test if sensitivity to shear stress of GPR68 is unique among GPCRs, we selected human GPCR clones that are considered mechanosensitive, including angiotensin II receptor type 1 (AGTR1), arginine vasopressin

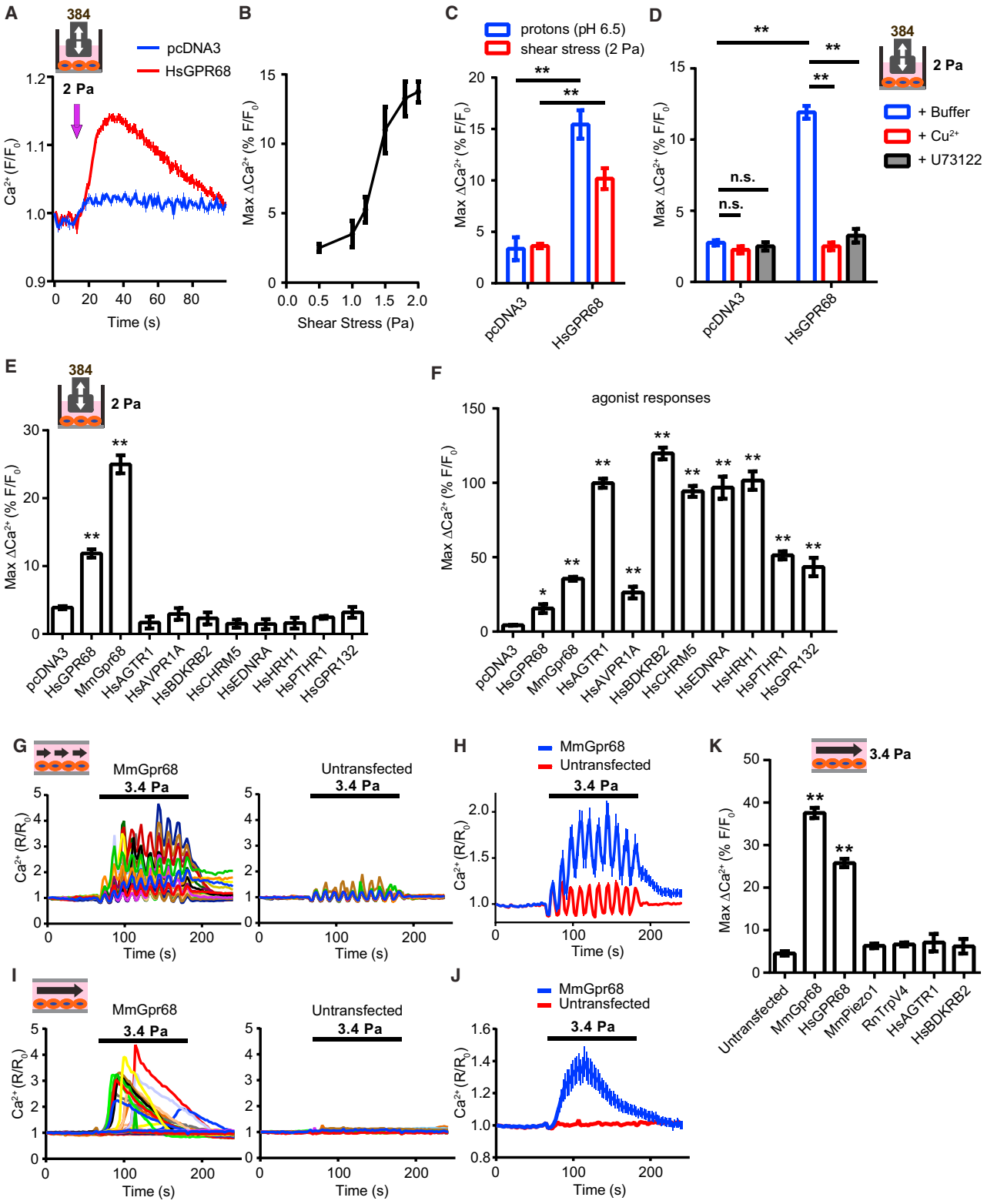

Figure 4. GPR68 Is Sensitive to Shear Stress Imposed by Both Disturbed and Laminar Flow in HEK293T Cells

(A) Disturbed flow-induced calcium transients in HEK293T cells transfected with human GPR68 or vector control 48 hr before the assay. Flow was applied at 60 Hz for 4 s (arrow indicates the onset of the flow).

(legend continued on next page)

receptor 1A (AVPR1A), BDKRB2, muscarinic cholinergic receptor 5 (CHRM5), endothelin receptor type A (EDNRA), histamine receptor H1 (HRH1), and PTHR1. These are $G_{q/11}$-coupled receptors that cause an increase in the intracellular calcium levels through the mobilization of calcium from intracellular stores upon activation. We transfected HEK293T cells with these GPCRs and subjected them to disturbed shear stress at 2 Pa. No significant increase in intracellular calcium levels was detected in cells transfected with GPCRs other than human GPR68. We demonstrated functional expression of these receptors by evaluating their response to known agonists (Figure 4F). Finally, we tested GPR132, the closest family member of GPR68 and also a $G_{q/11}$-coupled receptor, and found that it is not responsive to the same level of shear stress, while it did respond normally to its agonist lactate (Figures 4E and 4F) (Chen et al., 2017). These results highlight the unique sensitivity of GPR68 to disturbed shear stress.

Fluid flow *in vivo* can be laminar or disturbed. In laminar flow, the fluid flows in parallel layers in an orderly fashion (Chiu and Chien, 2011) and can be pulsatile or steady. In contrast, disturbed flow has irregular fluctuations with time and no clear direction. We tested if GPR68 responds to shear stress imposed by pulsatile laminar flow. With 1 Hz pulsatile laminar flow at 3.4 Pa, Gpr68-transfected HEK293T cells showed a robust increase of intracellular calcium levels. In most cells, the calcium level returned to baseline within minutes of the flow stopping. Non-transfected cells in the same chamber did not respond (Figures 4G and 4H). There were large, periodic fluctuations in calcium signals in both Gpr68-transfected cells and untransfected cells synchronous with the flow pulsatility. These are artifacts caused by the cyclic shift in optical focus as a result of the expansion and contraction of the plastic flow chamber in response to the pulsatile flow. We also assayed the cells' response to steady laminar flow. Robust responses were also observed with steady laminar flow in the transfected cells, but not in the non-transfected cells (Figures 4I and 4J).

Several proteins that are implicated as sensors of laminar flow, including TRPV4, PIEZO1, AGTR1, and BDKRB2 (Chachisvilis et al., 2006; Li et al., 2014; Mendoza et al., 2010; Ramkhelawon et al., 2013). None of those caused any significant increase in calcium levels with the same flow stimulation when expressed in HEK cells (Figure 4K).

GPR68 Is Expressed in Endothelial Cells of Small-Diameter Arteries

GPR68 is evolutionally conserved among vertebrates. No orthologs are found in bacteria, fungi, plants, or invertebrates. In mice, Gpr68 mRNA is detected in a variety of tissues (Figure 5A). The expression level is highest in the spleen, consistent with previous reports that Gpr68 transcripts are enriched in immune cells (Yan et al., 2014). We tested a number of commercially available or custom-made antibodies and found that none of them can specifically detect the heterologously expressed GPR68. Therefore, we employed *in situ* hybridization to detect Gpr68 transcripts in mouse tissue sections. Interestingly, we found that Gpr68 mRNA is detected in small-diameter blood vessels across a number of tissues, including pancreas, liver, and brain (Figure 5B). Based on morphology, the Gpr68+ cells appear to be endothelial cells. To determine the identity of those cells, we obtained an enhanced GFP (eGFP) reporter line of Gpr68 generated by the GenSat Project (Figure 5C). We first tested if the eGFP reporter faithfully represents endogenous Gpr68 expression. We isolated immune cells from the spleen of the reporter mice and C57 B/L6 mice and subjected them to fluorescence-activated cell sorting (FACS). GFP signal was detected in most CD8+ T cells, NK cells, and a subset of CD4+ cells. No GFP signal was detected in B cells (Figure S3A). qRT-PCR of the RNA isolated from sorted cells of C57 B/L6 mice showed that Gpr68 transcript levels are high in CD8+ T cells and NK cells, intermediate in CD4+ cells, and absent in B cells (Figure S3B). These results indicate that the GFP signal accurately represents endogenous Gpr68 transcription. Next, we tested if GFP signal is detected in endothelial cells. We isolated primary vascular endothelial cells from the mouse bladder and sorted cells that are positive for CD31 (endothelial cells) and negative for CD45 (leukocytes). We observed both GFP+ and GFP− populations of endothelial cells (Figure 5D [green and gray population, respectively]). RNA sequencing (RNA-seq) with GFP+ and GFP− endothelial cells showed that Gpr68 transcripts are enriched nearly 8-fold in GFP+ cells. In comparison, Piezo1 is expressed at similar levels across the two populations. These results validate that GFP levels accurately represent endogenous Gpr68 expression in endothelial cells.

We next evaluated Gpr68 expression pattern by staining a panel of tissue sections from eGFP reporter mice using a

(B) Quantification of the amplitude of the calcium transients evoked by disturbed shear stress of increasing intensities. n = 3 wells per intensity tested.
(C) Response of HEK293T cells to pH 6.5 stimulation and 2 Pa disturbed shear stress. **$p < 0.01$.
(D) Response of HEK293T cells to 2 Pa disturbed flow in the presence of 20 μM Cu^{2+} or 10 μM U73122. Cu^{2+} or U73122 was added to the assay buffer 2 min prior to the start of the flow. n.s., not significant. **$p < 0.01$.
(E) The shear stress induced responses of HEK293T cells transiently transfected with various human and mouse GPCRs. **$p < 0.01$.
(F) The agonist response of HEK293T cells transiently transfected with various human and mouse GPCRs. **$p < 0.01$. The chemical activators used were: pH 6.5 for human and murine GPR68, 0.5 μM angiotensin II for AGTR1, 0.5 μM [Arg^8]-vasopressin for AVPR1A, 0.5 μM bradykinin for BDKRB2, 0.5 μM acetylcholine chloride for CHRM5, 0.5 μM endothelin I for EDNRA, 0.5 μM histamine dihydrochloride for HRH1, 20 μM parathyroid hormone (1–34) for PTHR1, and 100 mM lactate for GPR132.
(G) Representative traces of intracellular calcium levels in HEK293T cells transfected with mouse Gpr68-IRES-eGFP upon pulsatile laminar flow stimulation. Cells with GFP signal were considered transfected and the GFP negative ones were untransfected. Pulsatile laminar flow was applied at 3.4 Pa, 1 Hz for 120 s.
(H) Quantification of the response of HEK cells to pulsatile laminar flow. n = 172 for MmGpr68 transfected and 165 for untransfected.
(I) Representative traces of intracellular calcium levels in HEK293T cells transfected with mouse Gpr68-IRES-eGFP upon steady laminar flow stimulation. Steady laminar flow was applied at 3.4 Pa for 120 s.
(J) Response of HEK cells to steady laminar flow. n = 162 for MmGpr68 transfected and 183 for untransfected.
(K) Responses of HEK293T cells transfected with various putative mechanosensors to steady laminar flow at 3.4 Pa. **$p < 0.01$.

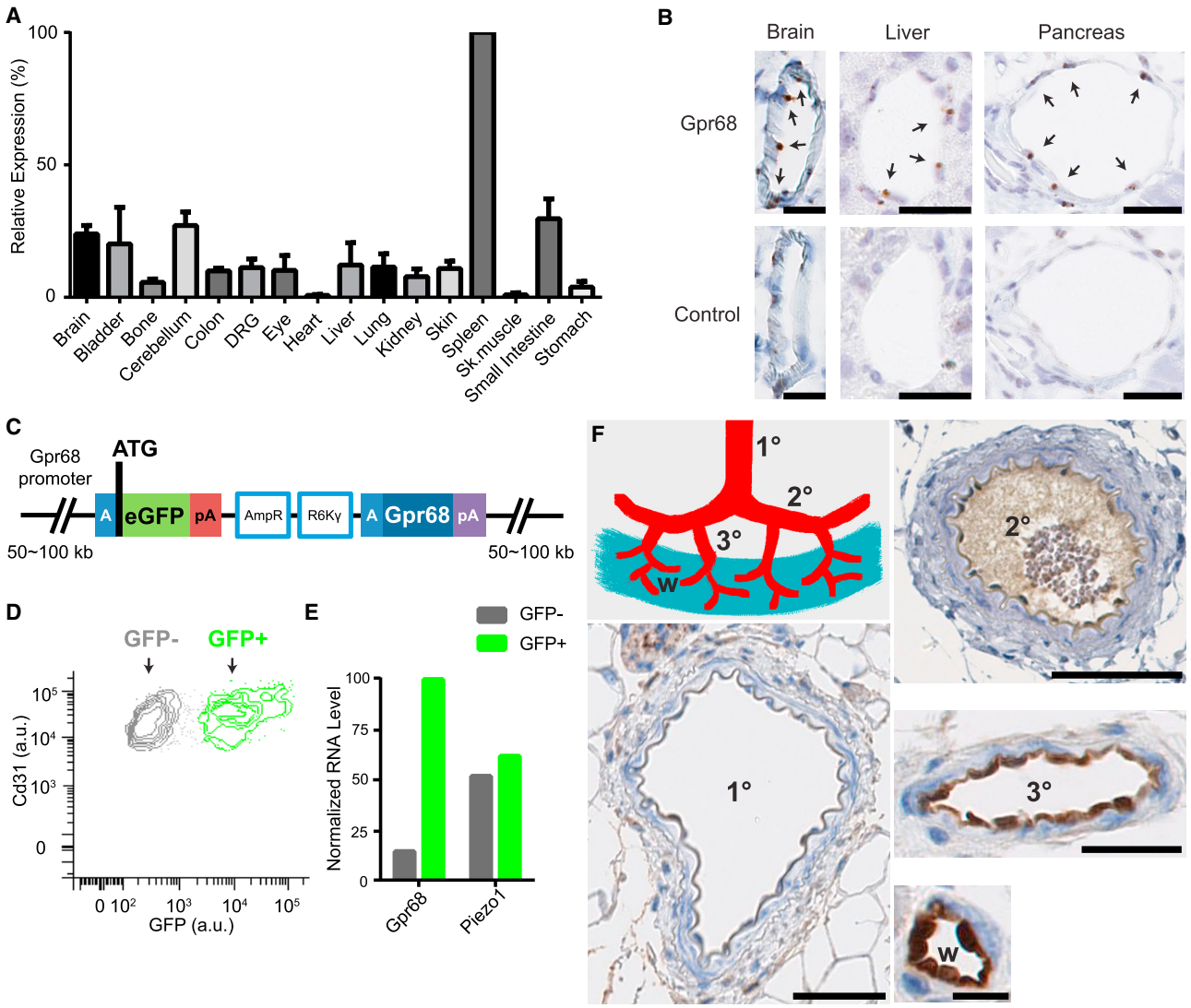

Figure 5. GPR68 Expression Is Detected in Endothelial Cells of Small-Diameter Vessels

(A) Murine Gpr68 mRNA expression profile determined by qRT-PCR. Gapdh was used as the reference gene. The expression levels were normalized to spleen. n = 2–3.

(B) Representative images of colorimetric RNAscope *in situ* hybridization for Gpr68 vascular endothelial cells of small-diameter blood vessels in brain, pancreas, and liver. Scale bars: 25 μm. Arrows indicate cells with positive signal.

(C) Schematic diagram of the bacterial artificial chromosome (BAC) transgenic construct that is integrated in the genome of Gpr68 eGFP reporter mice. The blue A box is the homologous sequence that guides recombination and insert eGFP after the start codon of Gpr68. Poly-A sequence following the eGFP blocks the transcription of the downstream genes within the construct (including Gpr68). pA: poly-A sequence; AmpR, amplicilin-resistance genes; R6Kγ, origin of DNA replication (AmpR and R6Kγ are used in the initial selection of BAC constructs).

(D) FACS plot of primary endothelial cells isolated from the bladder of Gpr68-eGFP reporter mice. Cells that are CD31+ and CD45− are shown and grouped in the GFP+ and GFP− populations.

(E) Normalized RNA levels (RPKM, reads per kilobase region) of Gpr68 and Piezo1 from the RNA-seq data of GFP+ and GFP− endothelial cells. Bladder cells from three batches of isolation and sorting (10 mice in total) were pooled and subjected to RNA-seq.

(F) Representative images of GFP antibody staining in arteries of first-order (1°), second-order (2°), and third-order (3°) superior mesenteric vessels and the vessels in the wall of small intestine (w). Scale bars: 50 μm for 1° and 2° vessels, 25 μm for 3° vessels, and 10 μm for vessels in the small intestine wall. Eight groups of vessels from four mice were examined.

See also Figure S3.

GFP antibody. The antibody stains endothelial cells in pancreas, liver, and bladder, among other tissues (Figures S3C–S3E). Consistent with the FACS result, we detected GFP only in a subset of endothelial cells (Figures S3D and S3E). Interestingly, the GFP+ cells appear to be endothelial cells of arterioles, the small-diameter arteries surrounded by

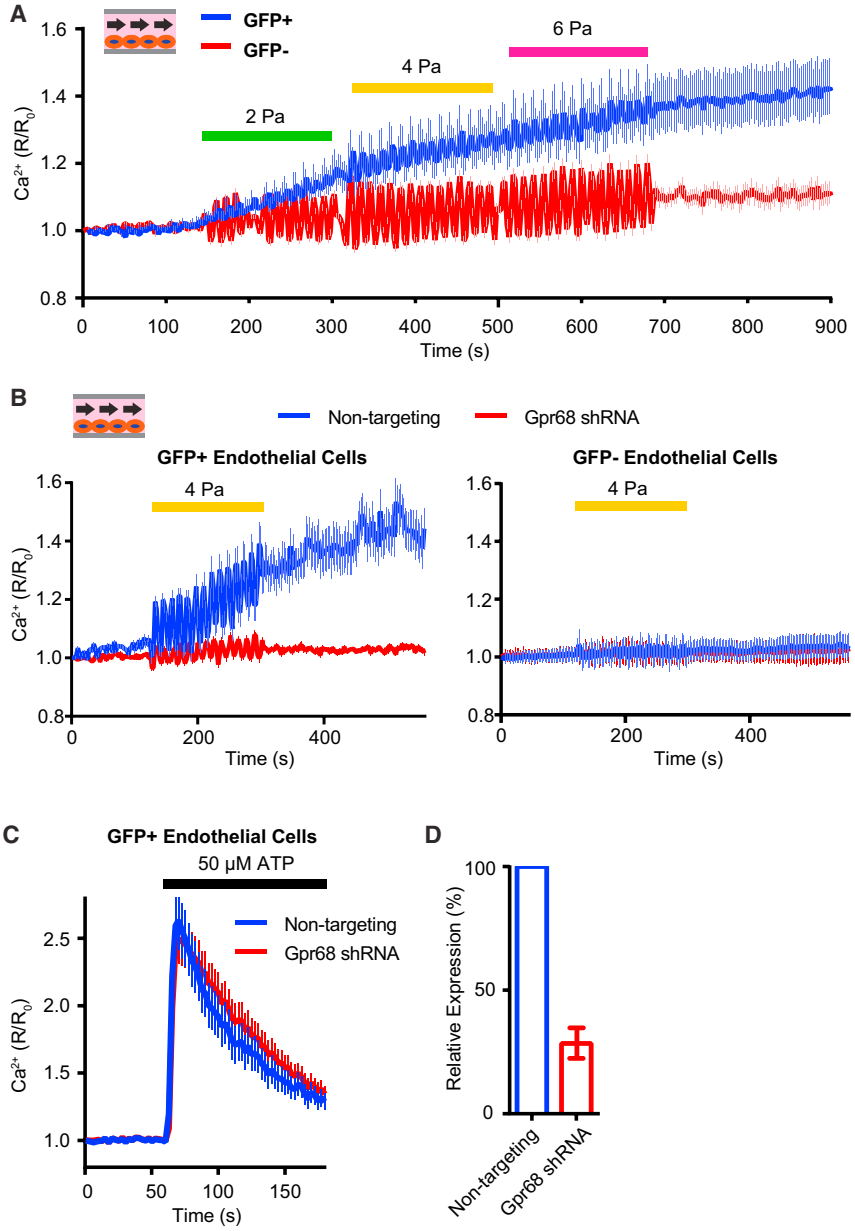

Figure 6. Gpr68 Is Necessary for Laminar Flow-Induced Calcium Transients in Murine Primary Microvascular Endothelial Cells

(A) Responses of mouse primary microvascular endothelial cells (MVECs) to shear stress imposed by pulsatile laminar flow with increasing amplitudes. The MVECs were isolated from cerebrum of the Gpr68 eGFP reporter mice. Pulsatile laminar flows of different amplitudes are applied at 1 Hz for 180 s. n = 148 (GFP+) and 155 (GFP−). Data are pooled from three trials.

(B) Responses of GFP+ and GFP− MVECs to pulsatile laminar shear stress at 4 Pa. The MVECs were infected with lentivirus containing non-targeting shRNA or Gpr68 shRNA constructs. The pulsatile flow is applied at 1 Hz for 180 s. n = 166 (non-targeting) and 173 (Gpr68 shRNA). Three trials.

(C) The calcium transients in primary MVECs induced by to 50 μM ATP. n = 223 (non-targeting) and 198 (Gpr68 shRNA). Three trials.

(D) Quantification of the knockdown efficiency of lentiviral shRNA against Gpr68. n = 3.

a layer of relatively thick smooth muscles. The venules, which have a less prominent smooth muscle layer, are mostly negative for GFP staining (Figures S3D and S3E). This is further confirmed by staining sections of mesenteric vessels. The GFP signal was not detected in first- and second-order arteries. The endothelial cells of third-order arterioles and the arterioles in the wall of small intestine showed the strongest GFP antibody staining (Figure 5F). These results indicate that Gpr68 is preferentially expressed in small-diameter resistance arteries, the major sites of regulation of resistance to blood flow, suggesting that Gpr68 may play a role in flow-mediated vasodilation.

GPR68 Is Required for Laminar Shear Stress Responses of Mouse Primary Microvascular Endothelial Cells

The striking expression pattern of Gpr68 predicts that the GFP+ endothelial cells should respond to shear stress. To test this, we isolated primary microvascular endothelial cells (MVECs) from the cerebrum of homozygous Gpr68-eGFP reporter mice and assayed their response to shear stress in the flow chamber. 1 Hz pulsatile laminar flow was applied with increasing intensity of 2 Pa, 4 Pa, and 6 Pa (physiologically relevant levels of shear stress experienced by small arteries). GFP+ endothelial cells responded to the flow by increasing intracellular calcium levels, while the GFP− cells showed significantly lower responses (Figure 6A). To test if the flow response is dependent on Gpr68, we carried out knockdown experiments with viruses containing Gpr68 small hairpin RNA (shRNA) and non-targeting shRNA. Upon stimulation with pulsatile flow at 4 Pa, the GFP+ cells infected with non-targeting shRNA virus showed an increase in intracellular calcium levels, while cells infected with Gpr68 shRNA virus showed no appreciable responses (Figure 6B). Importantly, GFP+ cells infected with either virus showed similar response to 50 μM ATP, demonstrating that these cells are healthy and able to respond to chemical stimuli (Figure 6C). qRT-PCR demonstrated that the RNA level of Gpr68 was knocked down by 73% in the Gpr68 shRNA-treated endothelial cells, compared to the non-targeting shRNA-treated cells (Figure 6D). These results show that the endogenous Gpr68 in primary MVECs is necessary for flow-induced calcium transients.

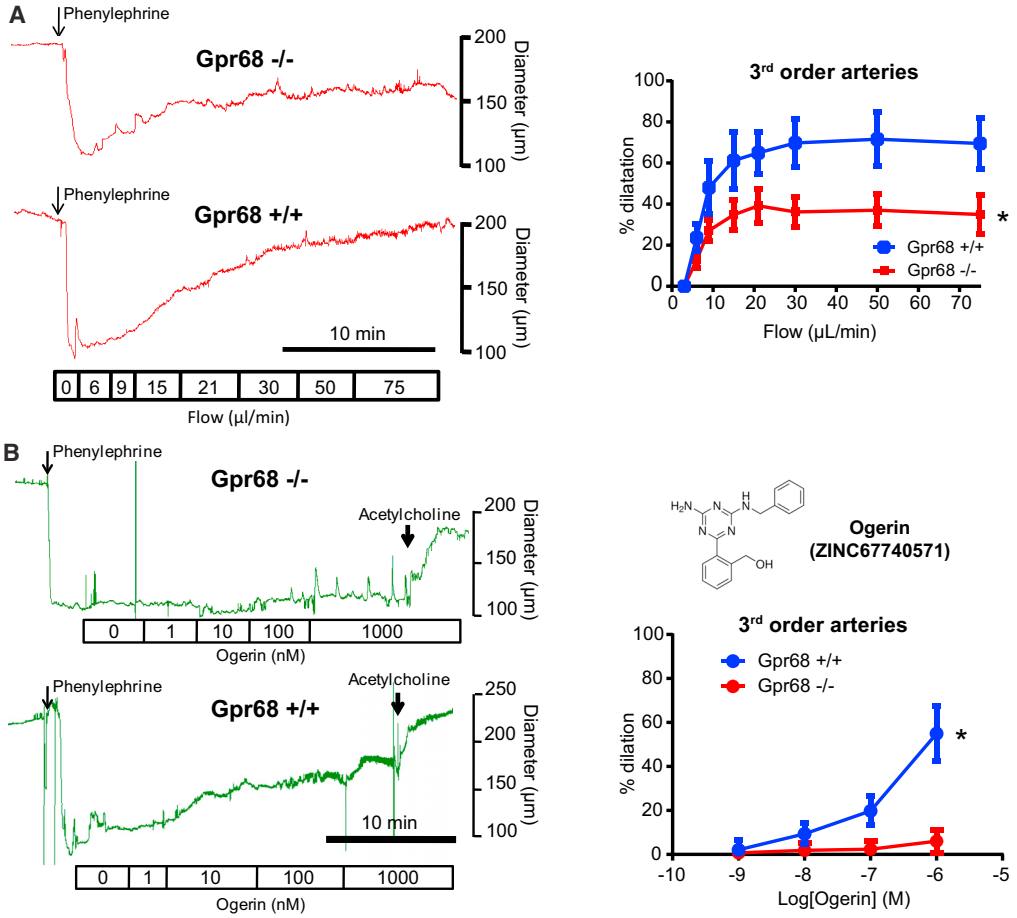

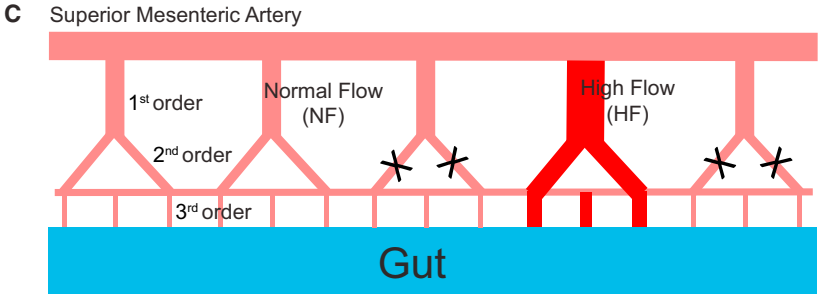

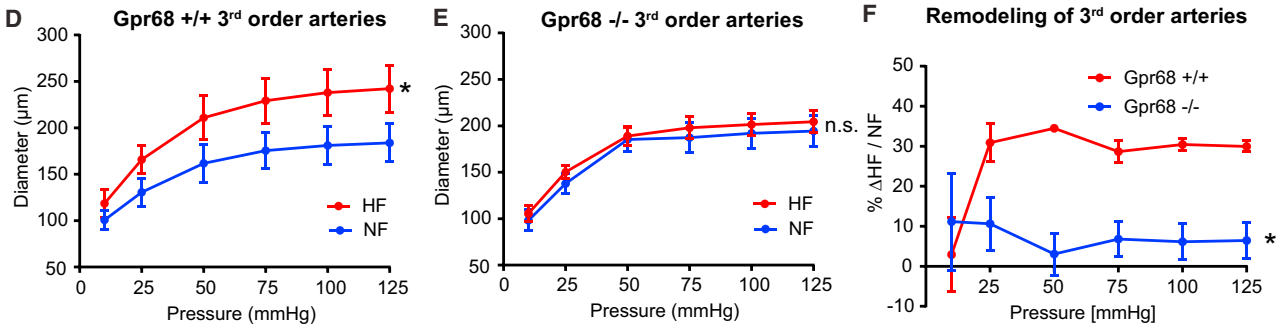

(legend on next page)

Gpr68 Is Required for Flow-Mediated Dilation of Mouse Small-Diameter Mesenteric Arteries *Ex Vivo*

The endothelial cells in resistance arteries sense increase in blood flow and signal to smooth muscles via nitric oxide (NO), endothelium-derived hyperpolarizing factor (EDHF), and other mechanisms to cause their relaxation (Niebauer and Cooke, 1996). This results in an increase in the diameter of the vessel and is called flow-mediated dilation (FMD). To investigate whether GPR68 is responsible for FMD, we isolated mesenteric arteries (MAs) from the Gpr68 knockout (KO, Gpr68 −/−) mice and performed *ex vivo* cannulation experiments. Compared to wild-type (WT, Gpr68 +/+) littermates, Gpr68 KO mice had significantly lower FMD response in third-order MAs (Figure 7A) but not in first- and second-order MAs (Figures S4A and S4B). This matches the expression pattern of Gpr68 in the mesenteric vessel bed (Figure 5F). Nitric oxide synthase (NOS) inhibitor L-NAME almost completely abolished FMD response in third-order MAs of both KO and WT animals, indicating that Gpr68 likely functions upstream of the NO pathway (Figure S4C). Notably, in third-order MAs, dilation to acetylcholine and constriction to KCl were similar between KO and WT mice (Figure S4D), indicating that loss of Gpr68 activity specifically affects the mechanical aspect of the dilation response in third-order MAs.

Since loss of Gpr68 activity leads to impaired FMD response in third-order MAs, we predicted that activating Gpr68 by chemical means only (i.e., without flow) would lead to vessel dilation. We synthesized an allosteric modulator of GPR68 named ogerin, which was shown to specifically modulate human and mouse GPR68 activity (Huang et al., 2015). We found that ogerin activates Gpr68 expressed in HEK293T cells, with an EC_{50} around 0.17 μM (Figure S5). Consistent with our prediction, adding ogerin to third-order WT MAs induced a dose-dependent dilation (Figure 7B). Importantly, similar vessels from KO mice displayed no dilation response to ogerin across a concentration range from 1 nM to 1 μM (Figure 7B).

Gpr68 KO mice are grossly normal (Yan et al., 2014). Our echocardiography study showed that they have similar cardiac parameters compared to WT littermates (Figure S6A). We also measured hemodynamic parameters in Gpr68 KO mice and found slightly lower systolic pressure, while diastolic pressure, mean arterial pressure, and heart rate were indistinguishable from WT mice (Figure S6B). The marginally lower systolic blood pressure phenotype could be due to compensatory mechanisms, which might cause a lowering of the baseline vascular tone or an increase in the effectiveness of alternative dilation mechanisms. Indeed, we found that the myogenic tone was lower in third-order arteries from Gpr68 KO mice (Figure S6C). In addition, the dilation response to nitric oxide donor sodium nitroprusside (SNP) is higher in KO vessels, suggesting that KO mice could be more sensitive to NO-induced vasodilation (Figure S6D).

GPR68 Is Required for Flow-Mediated Outward Remodeling of Mouse Small-Diameter Mesenteric Arteries *In Vivo*

Chronic rise in flow induces a diameter increase in vessels, and this flow-mediated outward remodeling (FMR), driven by the rise in shear stress, has a major role in post-ischemic revascularization (Henrion et al., 1997). To test if GPR68 is required for FMR, we performed ligation of second-order mesenteric vessels to create a branch of arteries with high flow (HF, Figure 7C). We found that FMR was absent in third-order MAs isolated from GPR68 KO mice compared to WT mice, where the increase in flow induced a significant diameter increase (Figures 7D–7F). Importantly, FMR in first-order arteries of GPR68 KO mice was not different from that observed in WT mice (Figures S7A–S7C), suggesting GPR68's shear stress-sensing role is specific to small-diameter arteries (resistance arteries, where GPR68 is expressed).

DISCUSSION

GPR68 Is a Mechanosensor

To categorize a protein as a mechanosensor, several criteria should ideally be met: it must be expressed in the correct cells, it must be essential for the immediate signaling response of cells to the relevant force, and it can be activated by the relevant mechanical force when expressed in heterologous cells or reconstituted in lipid bilayers (Ernstrom and Chalfie, 2002). Here, we provide evidence that GPR68, a class A rhodopsin-like GPCR, satisfies all three criteria for a mechanosensor. Gpr68 is expressed in a subset of vascular endothelial cells that have a significant response to shear stress. It is required for shear stress sensitivity of endothelial cells. Finally, overexpressing human or murine GPR68 in naive HEK293T cells induces sensitivity to shear stress in response to physiologically relevant types of flow stimulations.

Compared to other putative mechanosensitive GPCRs tested, only GPR68 overexpression gives rise to detectable levels of calcium transients in response to disturbed and laminar shear stress assay at the frequency and intensity used here. It

Figure 7. Gpr68 Is Required for Flow-Mediated Dilation and Outward Remodeling in Third-Order Mesenteric Arteries

(A) Flow-mediated dilation (FMD) response of third-order MAs isolated from Gpr68 KO mice and WT littermates. Vessels were cannulated and pre-constricted using 1 μM phenylephrine and subjected to stepwise increases in flow rates. Left: representative recordings of vessel diameter change. Scale bar: 10 min. Right: quantification of FMD response in third-order MAs. p = 0.044, two-way ANOVA, n = 9 for Gpr68 KO and n = 7 for WT.

(B) Dilation responses of third-order MAs to ogerin. Vessels were cannulated and pre-constricted using 1 μM phenylephrine, and subjected to ogerin with increasing concentration. Left: representative recordings of vessel diameter change. Scale bar: 10 min. Right: quantification of ogerin-induced dilation third-order MAs. Vessels from 6 KO and 6 WT mice were tested. p = 0.018, two-way ANOVA. Inset: structure of ogerin.

(C) Schematic representation of the surgery applied to mesenteric arteries to create local high-flow (HF) and normal flow (NF) regions (see STAR Methods).

(D and E) Flow-mediated remodeling (FMR) of third-order mesenteric arteries isolated from WT (p = 0.0045) and Gpr68 KO (p = 0.95) mice.

(F) The extent of outward remodeling as indicated by the percentage of vessel diameter increase (*p = 0.0309). *p < 0.05, two-way ANOVA for repeated measures, n = 5 for Gpr68 KO and n = 7 for WT.

See also Figures S4, S5, S6, and S7.

is possible that the other GPCRs are mechanosensitive, and higher levels of shear stress or other forms of mechanical forces are required for their activation. Nevertheless, we could not find evidence in the literature that direct mechanical stimulation, rather than osmotic stress, can activate any of the aforementioned GPCRs to induce immediate downstream events (e.g., PIP_2 depletion, change in intracellular calcium levels). However, AGTR1 and other GPCRs are proposed to be sensitive to membrane stretch when assayed indirectly by electrophysiological recording from HEK cells co-expressing TRPC6 (Mederos y Schnitzler et al., 2008).

How does GPR68 sense shear stress? There are reports of BDKRB2 activation by shear stress (Chachisvilis et al., 2006). Using time-resolved fluorescence microscopy and fluorescence resonance energy transfer (FRET), conformational dynamics of the receptor was detected upon application of fluid shear stress. This suggests that GPCRs can indeed undergo conformational changes under fluid shear stress. GPR68 likely interacts with cytoskeleton to effectively sense and transduce tension, as the tensegrity model predicts that mechanical behavior of cells emerges by interactions among different cytoskeletal filaments and extracellular adhesions (Wang et al., 2001). It is also possible that an unknown upstream mechanosensor can activate GPR68; however, this factor would be expressed quite ubiquitously.

Role of GPR68 in Endothelial Cells

It is interesting that both PIEZO1 and GPR68 are expressed in endothelial cells. However, we did not detect PIEZO1 activation by calcium imaging upon laminar flow (Figure 4K), although PIEZO1-dependent calcium transients were recorded in response to disturbed shear stress. This difference could be due to the fast inactivation of PIEZO1 when heterologously expressed. Unlike PIEZO1, activation of GPR68 causes a robust calcium release from intracellular stores in response to both laminar and disturbed flows. Importantly, GPR68-dependent mechanoresponses are present in MDA-MB-231, even when PIEZO1 is knocked down, indicating that the two can function independently (Figure 2D). Indeed, PIEZO1 is required for embryonic arterial remodeling, and its deletion causes embryonic lethality, while Gpr68-deficient mice survive to adulthood and are grossly normal (Li et al., 2009b). Given that PIEZO1 has also been recently implicated to play a role in FMD (Wang et al., 2016), as well as flow-stimulated vasoconstriction through endothelium-smooth muscle coupling (Rode et al., 2017), it is possible that both PIEZO1 and GPR68 contribute to sensing shear stress within endothelial cells. Analysis of double KO mice could shed light on whether PIEZO1 and GPR68 play additive/overlapping roles in endothelial cells.

GPR68 can also be activated by protons. Low pH and shear stress are both relevant stimuli that endothelial cells experience *in vivo*. Both acidosis (blood pH ~7.0) and shear stress cause acute vasodilation (Lindauer et al., 2003; Niebauer and Cooke, 1996), raising the possibility that GPR68 could be a polymodal receptor for the two distinct stimuli. Coincidence activation of GPR68 by proton and shear stress could endow GPR68 with the capacity to generate complex responses to these two physiologically relevant stimuli.

As a $G_{q/11}$-coupled receptor, GPR68 activation is expected to lead to the cleavage of PIP_2 into IP_3 and diacylglycerol (DAG) by PLC and induces calcium release from the store. In endothelial cells, this could trigger several acute signaling pathways, including the activation of Ca^{2+}-gated channels (ORAI1, $K_{Ca}2.3$, K_{Ca} 3.1) or synthesis of NO by NOS or release of EDHF (Grgic et al., 2009). Depletion of membrane-bound PIP_2 may also activate potassium channel subfamily K (KCNK) channels and lead to the hyperpolarization of the cells (Pathan and Rusch, 2011). The release of NO and EDHF and activation of KCNK channels in turn can lead to hyperpolarization of smooth muscles surrounding the vessels, causing them to relax and therefore dilate the vessels. We have shown that NO is likely an essential downstream pathway of GPR68 and leads to vasodilation (Figure S4C). Future studies might reveal additional pathways that could be activated by GPR68.

Role of GPR68 in Shear Stress Sensing *In Vivo*

We demonstrate that GPR68 is essential for FMD *ex vivo*, and FMR of small arteries *in vivo*. FMD is an acute dilatory response of the endothelium involved in tissue perfusion when the blood flow rate rises with increase in metabolic demand (Joyner and Casey, 2015; Levy et al., 2008). However, FMD does not necessarily correlate with systemic blood pressure. Indeed, in several mouse models without vimentin (Henrion et al., 1997) or dystrophin (Loufrani et al., 2001), FMD is selectively reduced with little change in blood pressure. Regardless, compromised flow-mediated dilation is considered to be a sign of endothelial dysfunction as observed in diseases related to vascular function. Given the requirement of GPR68 for FMD, it would be interesting to test whether the GPR68-deficient mice are prone to develop preclinical equivalent of hypertension, obesity, or diabetes when challenged.

FMR is governed by the rise in shear stress exerted on the endothelial cells and leads to the outward growth of the vascular wall and increased diameter so that shear stress is normalized over time. FMR plays a major role in collateral artery growth, or arteriogenesis, which is crucial to improve collateral circulation and tissue perfusion in patients with ischemic diseases. FMR becomes progressively reduced in aging (Dumont et al., 2008), is decreased even earlier in rat models of hypertension (Tuttle et al., 2002) and diabetes (Freidja et al., 2012), and has a strong prognostic significance in patients (Lynch et al., 2012). New therapeutics that improve FMR would potentially bring significant benefit to patients suffering from severe ischemia, as this would accelerate collateral artery growth and thus reperfusion (Silvestre et al., 2013).

Role of GPR68 in Other Cells

GPR68 is also expressed in a few other cell types, including neurons in the brain and dorsal root ganglia (DRG) and in leukocytes. We detected murine Gpr68 RNA in a subset of DRG neurons by *in situ* hybridization (data not shown). However, it is unlikely that GPR68 is the sensor underlying the mechanically activated currents observed in DRG neurons. All mechanically activated currents in DRG neurons have fast sub-millisecond onset (Delmas et al., 2011). In comparison, the fastest-signaling GPCRs described to date are the ones involved in photosensing, which

require at least 30–50 ms to activate and to couple to downstream ion channels (Burns and Pugh, 2010). GPR68 could serve as a modulator of other ion channels in DRG, similar to muscarinic acetylcholine receptors that modulate inward-rectifying K^+ channels (Chuang et al., 1997). GPR68 is also highly expressed in immune cells. It has been suggested that the expression of Gpr68 in myeloid-derived cells is required for prostate cancer cell-induced immunosuppression (Yan et al., 2014). GPR68 mice also have impaired T cell responses associated with a reduced frequency and number of dendritic cells (DCs), higher production of nitric oxide by macrophages, and defects in DCs migration to draining lymph nodes (Aoki et al., 2013; D'Souza et al., 2016). There's also evidence suggesting that GPR68 could be involved in recall of fear conditioning in mice (Huang et al., 2015). Interestingly, it is suggested that GPR68 as a proton sensor is required for proper enamel formation in humans, although the KO mice lack the enamel formation phenotype (Parry et al., 2016). The mechanism of these effects, and whether mechanotransduction is involved in these various processes, is not clear.

Significance of the High-Throughput Mechanical Assay System and Identification of GPR68

Our high-throughput shear stress stimulation system vastly improves the throughput of mechanotransduction assays. This enabling technology has made unbiased, genome-wide screens for novel mechanosensitive proteins and pathways feasible. The identification of GPR68 as a novel mechanosensor validates the value and potential of this innovative system and expands the repertoire of membrane proteins that sense mechanical forces *in vivo*.

STAR★METHODS

Detailed methods are provided in the online version of this paper and include the following:

- KEY RESOURCES TABLE
- CONTACT FOR REAGENT AND RESOURCE SHARING
- EXPERIMENTAL MODEL AND SUBJECT DETAILS
  - Animals
  - Cell lines and cell culture
- METHOD DETAILS
  - Constructs and Compounds
  - Engineering
  - Cell-based Experiments
  - In Vivo Experiments
  - Miscellaneous
- QUANTIFICATION AND STATISTICAL ANALYSIS
- DATA AND SOFTWARE AVAILABILITY

SUPPLEMENTAL INFORMATION

Supplemental Information includes seven figures and can be found with this article online at https://doi.org/10.1016/j.cell.2018.03.076.

ACKNOWLEDGMENTS

We thank Alec Wilson, Ton Trinh, and Hai Nguyen for engineering support; Sungjoon Kim for supplying human cancer cells; Craig Mickanin for picking the siRNA library; Yufeng Zhai and Yingyao Zhou for help with siRNA screen data analysis; Zhaozhu Qiu, Buu Tu, Loren Miraglia, Sanjeev Ranade, Angelica Romero, Glenn Federe, James Watson, Teri Johnson, Rita Moran and Kathryn Spencer for assistance; and members of Patapoutian group for constructive discussions. This work was partly supported by a grant from the NIH (NIH R01 #DE022358 to A.P.). A.P. is an investigator of the Howard Hughes Medical Institute.

AUTHOR CONTRIBUTIONS

J.X. and A.P. initiated the project and designed experiments. J.X., S.H., and J.K.M. designed and constructed the shear stress stimulation systems. J.X. performed the experiments with the assistance of J.M., K.N., M.P., A.F., V. Lee, F.-I.X., S.M.C., S.M., V. Lukacs, L.B., and M.B. E.V., J.F., and L.G. performed vessel cannulation experiments. J.L. performed echocardiogram analysis. A.P.O. conducted bioinformatics analysis and picked the siRNA library with 2+TM genes. J.R.W. performed RNa-seq analysis. Y.X. provided Gpr68 KO mice. J.X., M.B., D.H., and A.P. analyzed the data. J.X. and A.P. wrote the manuscript. J.X., B.L., S.C., D.H., and A.P. revised the manuscript. A.P. supervised the project.

DECLARATION OF INTERESTS

The authors declare no competing interests.

Received: July 7, 2017
Revised: December 21, 2017
Accepted: March 27, 2018
Published: April 19, 2018

REFERENCES

Aoki, H., Mogi, C., Hisada, T., Nakakura, T., Kamide, Y., Ichimonji, I., Tomura, H., Tobo, M., Sato, K., Tsurumaki, H., et al. (2013). Proton-sensing ovarian cancer G protein-coupled receptor 1 on dendritic cells is required for airway responses in a murine asthma model. PLoS ONE *8*, e79985.

Burns, M.E., and Pugh, E.N., Jr. (2010). Lessons from photoreceptors: turning off g-protein signaling in living cells. Physiology (Bethesda) *25*, 72–84.

Caillon, A., Grenier, C., Grimaud, L., Vessieres, E., Guihot, A.L., Blanchard, S., Lelievre, E., Chabbert, M., Foucher, E.D., Jeannin, P., et al. (2016). The angiotensin II type 2 receptor activates flow-mediated outward remodelling through T cells-dependent interleukin-17 production. Cardiovasc. Res. *112*, 515–525.

Chachisvilis, M., Zhang, Y.L., and Frangos, J.A. (2006). G protein-coupled receptors sense fluid shear stress in endothelial cells. Proc. Natl. Acad. Sci. USA *103*, 15463–15468.

Chen, P., Zuo, H., Xiong, H., Kolar, M.J., Chu, Q., Saghatelian, A., Siegwart, D.J., and Wan, Y. (2017). Gpr132 sensing of lactate mediates tumor-macrophage interplay to promote breast cancer metastasis. Proc. Natl. Acad. Sci. USA *114*, 580–585.

Chiu, J.J., and Chien, S. (2011). Effects of disturbed flow on vascular endothelium: pathophysiological basis and clinical perspectives. Physiol. Rev. *91*, 327–387.

Chuang, H., Jan, Y.N., and Jan, L.Y. (1997). Regulation of IRK3 inward rectifier K+ channel by m1 acetylcholine receptor and intracellular magnesium. Cell *89*, 1121–1132.

Coste, B., Mathur, J., Schmidt, M., Earley, T.J., Ranade, S., Petrus, M.J., Dubin, A.E., and Patapoutian, A. (2010). Piezo1 and Piezo2 are essential components of distinct mechanically activated cation channels. Science *330*, 55–60.

D'Souza, C.A., Zhao, F.L., Li, X., Xu, Y., Dunn, S.E., and Zhang, L. (2016). OGR1/GPR68 Modulates the Severity of Experimental Autoimmune Encephalomyelitis and Regulates Nitric Oxide Production by Macrophages. PLoS ONE *11*, e0148439.

Delmas, P., Hao, J., and Rodat-Despoix, L. (2011). Molecular mechanisms of mechanotransduction in mammalian sensory neurons. Nat. Rev. Neurosci. *12*, 139–153.

Driscoll, M., and Chalfie, M. (1991). The mec-4 gene is a member of a family of Caenorhabditis elegans genes that can mutate to induce neuronal degeneration. Nature *349*, 588–593.

Dumont, O., Pinaud, F., Guihot, A.L., Baufreton, C., Loufrani, L., and Henrion, D. (2008). Alteration in flow (shear stress)-induced remodelling in rat resistance arteries with aging: improvement by a treatment with hydralazine. Cardiovasc. Res. *77*, 600–608.

Ernstrom, G.G., and Chalfie, M. (2002). Genetics of sensory mechanotransduction. Annu. Rev. Genet. *36*, 411–453.

Freidja, M.L., Tarhouni, K., Toutain, B., Fassot, C., Loufrani, L., and Henrion, D. (2012). The AGE-breaker ALT-711 restores high blood flow-dependent remodeling in mesenteric resistance arteries in a rat model of type 2 diabetes. Diabetes *61*, 1562–1572.

Grgic, I., Kaistha, B.P., Hoyer, J., and Köhler, R. (2009). Endothelial Ca+-activated K+ channels in normal and impaired EDHF-dilator responses–relevance to cardiovascular pathologies and drug discovery. Br. J. Pharmacol. *157*, 509–526.

Henrion, D., Terzi, F., Matrougui, K., Duriez, M., Boulanger, C.M., Colucci-Guyon, E., Babinet, C., Briand, P., Friedlander, G., Poitevin, P., and Lévy, B.I. (1997). Impaired flow-induced dilation in mesenteric resistance arteries from mice lacking vimentin. J. Clin. Invest. *100*, 2909–2914.

Huang, M., and Chalfie, M. (1994). Gene interactions affecting mechanosensory transduction in Caenorhabditis elegans. Nature *367*, 467–470.

Huang, X.P., Karpiak, J., Kroeze, W.K., Zhu, H., Chen, X., Moy, S.S., Saddoris, K.A., Nikolova, V.D., Farrell, M.S., Wang, S., et al. (2015). Allosteric ligands for the pharmacologically dark receptors GPR68 and GPR65. Nature *527*, 477–483.

Ishida, T., Takahashi, M., Corson, M.A., and Berk, B.C. (1997). Fluid shear stress-mediated signal transduction: how do endothelial cells transduce mechanical force into biological responses? Ann. N. Y. Acad. Sci *811*, 12–23.

Jaalouk, D.E., and Lammerding, J. (2009). Mechanotransduction gone awry. Nat. Rev. Mol. Cell Biol. *10*, 63–73.

Joyner, M.J., and Casey, D.P. (2015). Regulation of increased blood flow (hyperemia) to muscles during exercise: a hierarchy of competing physiological needs. Physiol. Rev. *95*, 549–601.

Käll, L., Krogh, A., and Sonnhammer, E.L. (2004). A combined transmembrane topology and signal peptide prediction method. J. Mol. Biol. *338*, 1027–1036.

Käll, L., Krogh, A., and Sonnhammer, E.L. (2007). Advantages of combined transmembrane topology and signal peptide prediction–the Phobius web server. Nucleic Acids Res. *35*, W429–W432.

Kang, L., Gao, J., Schafer, W.R., Xie, Z., and Xu, X.Z. (2010). C. elegans TRP family protein TRP-4 is a pore-forming subunit of a native mechanotransduction channel. Neuron *67*, 381–391.

Levina, N., Tötemeyer, S., Stokes, N.R., Louis, P., Jones, M.A., and Booth, I.R. (1999). Protection of Escherichia coli cells against extreme turgor by activation of MscS and MscL mechanosensitive channels: identification of genes required for MscS activity. EMBO J. *18*, 1730–1737.

Levy, B.I., Schiffrin, E.L., Mourad, J.J., Agostini, D., Vicaut, E., Safar, M.E., and Struijker-Boudier, H.A. (2008). Impaired tissue perfusion: a pathology common to hypertension, obesity, and diabetes mellitus. Circulation *118*, 968–976.

Li, H., and Durbin, R. (2009). Fast and accurate short read alignment with Burrows-Wheeler transform. Bioinformatics *25*, 1754–1760.

Li, W., Feng, Z., Sternberg, P.W., and Xu, X.Z. (2006). A C. elegans stretch receptor neuron revealed by a mechanosensitive TRP channel homologue. Nature *440*, 684–687.

Li, H., Handsaker, B., Wysoker, A., Fennell, T., Ruan, J., Homer, N., Marth, G., Abecasis, G., and Durbin, R.; 1000 Genome Project Data Processing Subgroup (2009a). The Sequence Alignment/Map format and SAMtools. Bioinformatics *25*, 2078–2079.

Li, H., Wang, D., Singh, L.S., Berk, M., Tan, H., Zhao, Z., Steinmetz, R., Kirmani, K., Wei, G., and Xu, Y. (2009b). Abnormalities in osteoclastogenesis and decreased tumorigenesis in mice deficient for ovarian cancer G protein-coupled receptor 1. PLoS ONE *4*, e5705.

Li, J., Hou, B., Tumova, S., Muraki, K., Bruns, A., Ludlow, M.J., Sedo, A., Hyman, A.J., McKeown, L., Young, R.S., et al. (2014). Piezo1 integration of vascular architecture with physiological force. Nature *515*, 279–282.

Lindauer, U., Vogt, J., Schuh-Hofer, S., Dreier, J.P., and Dirnagl, U. (2003). Cerebrovascular vasodilation to extraluminal acidosis occurs via combined activation of ATP-sensitive and Ca2+-activated potassium channels. J. Cereb. Blood Flow Metab. *23*, 1227–1238.

Livak, K.J., and Schmittgen, T.D. (2001). Analysis of relative gene expression data using real-time quantitative PCR and the 2(-Delta Delta C(T)) Method. Methods *25*, 402–408.

Loufrani, L., Matrougui, K., Gorny, D., Duriez, M., Blanc, I., Lévy, B.I., and Henrion, D. (2001). Flow (shear stress)-induced endothelium-dependent dilation is altered in mice lacking the gene encoding for dystrophin. Circulation *103*, 864–870.

Ludwig, M.G., Vanek, M., Guerini, D., Gasser, J.A., Jones, C.E., Junker, U., Hofstetter, H., Wolf, R.M., and Seuwen, K. (2003). Proton-sensing G-protein-coupled receptors. Nature *425*, 93–98.

Lukacs, V., Mathur, J., Mao, R., Bayrak-Toydemir, P., Procter, M., Cahalan, S.M., Kim, H.J., Bandell, M., Longo, N., Day, R.W., et al. (2015). Impaired PIEZO1 function in patients with a novel autosomal recessive congenital lymphatic dysplasia. Nat. Commun. *6*, 8329.

Lynch, F.M., Izzard, A.S., Austin, C., Prendergast, B., Keenan, D., Malik, R.A., and Heagerty, A.M. (2012). Effects of diabetes and hypertension on structure and distensibilty of human small coronary arteries. J. Hypertens. *30*, 384–389.

Mederos y Schnitzler, M., Storch, U., Meibers, S., Nurwakagari, P., Breit, A., Essin, K., Gollasch, M., and Gudermann, T. (2008). Gq-coupled receptors as mechanosensors mediating myogenic vasoconstriction. EMBO J. *27*, 3092–3103.

Melchior, B., and Frangos, J.A. (2012). Gαq/11-mediated intracellular calcium responses to retrograde flow in endothelial cells. Am. J. Physiol. Cell Physiol. *303*, C467–C473.

Mendoza, S.A., Fang, J., Gutterman, D.D., Wilcox, D.A., Bubolz, A.H., Li, R., Suzuki, M., and Zhang, D.X. (2010). TRPV4-mediated endothelial Ca2+ influx and vasodilation in response to shear stress. Am. J. Physiol. Heart Circ. Physiol. *298*, H466–H476.

Navone, S.E., Marfia, G., Invernici, G., Cristini, S., Nava, S., Balbi, S., Sangiorgi, S., Ciusani, E., Bosutti, A., Alessandri, G., et al. (2013). Isolation and expansion of human and mouse brain microvascular endothelial cells. Nat. Protoc. *8*, 1680–1693.

Niebauer, J., and Cooke, J.P. (1996). Cardiovascular effects of exercise: role of endothelial shear stress. J. Am. Coll. Cardiol. *28*, 1652–1660.

Nonomura, K., Woo, S.H., Chang, R.B., Gillich, A., Qiu, Z., Francisco, A.G., Ranade, S.S., Liberles, S.D., and Patapoutian, A. (2017). Piezo2 senses airway stretch and mediates lung inflation-induced apnoea. Nature *541*, 176–181.

Parry, D.A., Smith, C.E., El-Sayed, W., Poulter, J.A., Shore, R.C., Logan, C.V., Mogi, C., Sato, K., Okajima, F., Harada, A., et al. (2016). Mutations in the pH-Sensing G-protein-Coupled Receptor GPR68 Cause Amelogenesis Imperfecta. Am. J. Hum. Genet. *99*, 984–990.

Pathan, A.R., and Rusch, N.J. (2011). Two-pore domain K^+ channels: evidence for TWIK-2 in blood pressure regulation. Hypertension *58*, 539–541.

Ramkhelawon, B., Rivas, D., and Lehoux, S. (2013). Shear stress activates extracellular signal-regulated kinase 1/2 via the angiotensin II type 1 receptor. FASEB J. *27*, 3008–3016.

Ranade, S.S., Qiu, Z., Woo, S.H., Hur, S.S., Murthy, S.E., Cahalan, S.M., Xu, J., Mathur, J., Bandell, M., Coste, B., et al. (2014). Piezo1, a mechanically activated ion channel, is required for vascular development in mice. Proc. Natl. Acad. Sci. USA *111*, 10347–10352.

Retailleau, K., Duprat, F., Arhatte, M., Ranade, S.S., Peyronnet, R., Martins, J.R., Jodar, M., Moro, C., Offermanns, S., Feng, Y., et al. (2015). Piezo1 in Smooth Muscle Cells Is Involved in Hypertension-Dependent Arterial Remodeling. Cell Rep. *13*, 1161–1171.

Rode, B., Shi, J., Endesh, N., Drinkhill, M.J., Webster, P.J., Lotteau, S.J., Bailey, M.A., Yuldasheva, N.Y., Ludlow, M.J., Cubbon, R.M., et al. (2017).

Piezo1 channels sense whole body physical activity to reset cardiovascular homeostasis and enhance performance. Nat. Commun. *8*, 350.

Schwaderer, A.L., and Schwartz, G.J. (2004). Back to basics: acidosis and alkalosis. Pediatr. Rev *25*, 350–357.

Silvestre, J.S., Smadja, D.M., and Lévy, B.I. (2013). Postischemic revascularization: from cellular and molecular mechanisms to clinical applications. Physiol. Rev. *93*, 1743–1802.

Storch, U., Mederos y Schnitzler, M., and Gudermann, T. (2012). G protein-mediated stretch reception. Am. J. Physiol. Heart Circ. Physiol. *302*, H1241–H1249.

Sukharev, S.I., Blount, P., Martinac, B., Blattner, F.R., and Kung, C. (1994). A large-conductance mechanosensitive channel in E. coli encoded by mscL alone. Nature *368*, 265–268.

Tuttle, J.L., Sanders, B.M., Burkhart, H.M., Fath, S.W., Kerr, K.A., Watson, W.C., Herring, B.P., Dalsing, M.C., and Unthank, J.L. (2002). Impaired collateral artery development in spontaneously hypertensive rats. Microcirculation *9*, 343–351.

Walker, R.G., Willingham, A.T., and Zuker, C.S. (2000). A Drosophila mechanosensory transduction channel. Science *287*, 2229–2234.

Wang, N., Naruse, K., Stamenović, D., Fredberg, J.J., Mijailovich, S.M., Tolić-Nørrelykke, I.M., Polte, T., Mannix, R., and Ingber, D.E. (2001). Mechanical behavior in living cells consistent with the tensegrity model. Proc. Natl. Acad. Sci. USA *98*, 7765–7770.

Wang, S., Chennupati, R., Kaur, H., Iring, A., Wettschureck, N., and Offermanns, S. (2016). Endothelial cation channel PIEZO1 controls blood pressure by mediating flow-induced ATP release. J. Clin. Invest. *126*, 4527–4536.

Woo, S.H., Ranade, S., Weyer, A.D., Dubin, A.E., Baba, Y., Qiu, Z., Petrus, M., Miyamoto, T., Reddy, K., Lumpkin, E.A., et al. (2014). Piezo2 is required for Merkel-cell mechanotransduction. Nature *509*, 622–626.

Yan, Z., Zhang, W., He, Y., Gorczyca, D., Xiang, Y., Cheng, L.E., Meltzer, S., Jan, L.Y., and Jan, Y.N. (2013). Drosophila NOMPC is a mechanotransduction channel subunit for gentle-touch sensation. Nature *493*, 221–225.

Yan, L., Singh, L.S., Zhang, L., and Xu, Y. (2014). Role of OGR1 in myeloid-derived cells in prostate cancer. Oncogene *33*, 157–164.

Zhang, Y.L., Frangos, J.A., and Chachisvilis, M. (2009). Mechanical stimulus alters conformation of type 1 parathyroid hormone receptor in bone cells. Am. J. Physiol. Cell Physiol. *296*, C1391–C1399.

STAR★METHODS

KEY RESOURCES TABLE

REAGENT or RESOURCE	SOURCE	IDENTIFIER
3D printer	3D Systems	Projet MJP 3500
UV-cured resin	3D Systems	Visijet
Neodymium subwoofer driver	Tang Band	W3-1750S
Miniature 3-axis accelerometer	Analog Devices	ADXL326
Amplifier	Crown	D-150A II
Data Acquisition Card	National Instruments	USB-6341
CMOS camera	Hamamatsu	ORCA-Flash 4.0
Ibidi pump system	Ibidi	10902
Antibodies		
Goat anti-GFP antibody	Lifespan Biosciences	LS-C67081
Rabbit anti-mouse Gpr68	Lifespan Biosciences	LS-A3968, LS-A1194
Rabbit anti-mouse Gpr68	Pierce Biotechnologies	N/A
Brilliant Violet 421 anti-mouse CD4	Biolegend	100437
Brilliant Violet 65 anti-mouse CD3	Biolegend	100229
APC/Cy7 anti-mouse CD19	Biolegend	115529
PerCP/Cy5.5 anti-mouse CD8	Biolegend	100733
APC anti-mouse NK-1.1	Biolegend	108709
APC-Cy7 Rat Anti-Mouse CD45	BD Bioscienes	557659
Bacterial and Virus Strains		
pLKO.1-Gpr68-TRC-shRNA	Dharmacon	RMM4534-EG238377
Biological Samples		
Mouse C57 Brain Total RNA	Zyagen	MR-201-C57
Mouse C57 Bladder Total RNA	Zyagen	MR-902-C57
Mouse C57 Bone Total RNA	Zyagen	MR-107-C57
Mouse C57 Cerebellum Total RNA	Zyagen	MR-202-C57
Mouse C57 Colon Total RNA	Zyagen	MR-311-C57
Mouse C57 Eye Total RNA	Zyagen	MR-106-C57
Mouse C57 Heart Total RNA	Zyagen	MR-801-C57
Mouse C57 Liver Total RNA	Zyagen	MR-314-C57
Mouse C57 Lung Total RNA	Zyagen	MR-601-C57
Mouse C57 Kidney Total RNA	Zyagen	MR-901-C57
Mouse C57 Skin Total RNA	Zyagen	MR-101-C57
Mouse C57 Spleen Total RNA	Zyagen	MR-701-C57
Mouse C57 Skeletal Muscle Total RNA	Zyagen	MR-102-C57
Mouse C57 Small Intestine Total RNA	Zyagen	MR-306-C57
Mouse C57 Stomach Total RNA	Zyagen	MR-302-C57
Chemicals, Peptides, and Recombinant Proteins		
Ogerin	WuXi AppTek	N/A
Angiotensin II	Tocris Bioscience	1158
[Arg^{8}]-Vasopressin	Tocris Bioscience	2935
Bradykinin	Tocris Bioscience	3004
Acetylcholine Chloride	Tocris Bioscience	2809
Endothelin 1	Tocris Bioscience	1160
Histamine Dihydrochloride	Tocris Bioscience	3545

(*Continued on next page*)

Continued

REAGENT or RESOURCE	SOURCE	IDENTIFIER
Parathyroid Hormone (1-34)	Tocris Bioscience	3011
Lactate	Sigma Aldrich	L7022
U73122	Tocris Bioscience	1268
Critical Commercial Assays		
Human GPR68 RT-PCR Assay	Life Technologies	Hs 00268858_s1
Mouse Gpr68 RT-PCR Assay	Life Technologies	Mm 00558545_s1
Human GPR68 RT-PCR Assay	IDT	Hs.PT.58.27651490.g
Mouse Gpr68 RT-PCR Assay	IDT	Mm.PT.58.42531755
Mouse Gpr68 RNAScope probe	ACDBio	319321
DapB RNAScope probe	ACDBio	310043
Deposited Data		
GPR68-eGFP primary mouse endothelial cell RNaseq data	This paper	https://www.ncbi.nlm.nih.gov/geo/query/acc.cgi?acc=GSE111784
Experimental Models: Cell Lines		
A549 (Lung, Male)	ATCC	CRM-CCL-185
C32 (Skin, Male)	ATCC	CRL-1585
COLO 205 (Colon, Male)	ATCC	CCL-222
GM2345 (Brain, N/A)	ATCC	Discontinued
GM2493 (Brain, NA)	ATCC	Discontinued
HCT 116 (Colon, Male)	ATCC	CCL-247
HT-1080 (Connective Tissue, Male)	ATCC	CCL-121
HT-29 (Colon, Female)	ATCC	HTB-38
HuH-7 (Liver, Male)	JCRB	0403
KPNYN (Brain, N/A)	ATCC	Discontinued
NCI-H226 (Lung, N/A)	ATCC	CRL-5826
NCI-H510 (Lung, N/A)	ATCC	HTB-184
OVCAR4 (Ovary, Female)	ATCC	Discontinued
PANC-1 (Pancreas, Male)	ATCC	CRL-1469
RPMI-7951 (Skin, Female)	ATCC	HTB-66
SH-SY5Y (Bone Marrow, Female)	ATCC	CRL-2266
SK-MEL-28 (Skin, Male)	ATCC	HTB-72
SK-MEL-5 (Skin, Female)	ATCC	HTB-70
SK-N-AS (Brain, Female)	ATCC	CRL-2137
SK-OV-3 (Ovary, Female)	ATCC	HTB-77
SN12C (Kidney, N/A)	ATCC	Discontinued
SW480 (Colon, Male)	ATCC	CCL-228
U251 (Brain, N/A)	ATCC	Discontinued
U2-OS (Bone, Female)	ATCC	HTB-96
MDA-MB-231 (Breast, Female)	ATCC	HTB-26
HEK293T (Kidney, Fetal)	ATCC	CRL-11268
HUVEC (Umbilical Vein, N/A)	ATCC	CRL-1730
Experimental Models: Organisms/Strains		
Gpr68 −/− mice (Gpr68$^{tm1.1Yaxu}$, C57BL/6J background)	Dr. Yan Xu, Indiana University School of Medicine	MGI ID: 3849457
Gpr68-eGFP reporter mice (Tg(Gpr68-EGFP)IU33Gsat/Mmucd)	GenSat Project, The Rockefeller University.	RRID: MMRRC_031057-UCD

(*Continued on next page*)

Continued

REAGENT or RESOURCE	SOURCE	IDENTIFIER
Oligonucleotides		
2TM+ human siRNA library	Novartis AG Internal Collection	N/A
Final reconfirmation On Target Plus (OTP) siRNA library, custom order	Dharmacon	N/A
PIEZO1 siRNA	Dharmacon	L-020870
ATP2A2 siRNA	Dharmacon	L-004082
GPR68 siRNA	Dharmacon	L-005591
Recombinant DNA		
Human GPR68 in pcDNA3.1+	Missouri S&T cDNA Resource Center	GPR0680000
Human GPR132 in pcDNA3.1+	Missouri S&T cDNA Resource Center	GPR1320000
Human AGTR1 in pcDNA3.1+	Missouri S&T cDNA Resource Center	AGTR100001
Human AVPR1A in pcDNA3.1+	Missouri S&T cDNA Resource Center	AVR01A0000
Human BDKRB2 in pcDNA3.1+	Missouri S&T cDNA Resource Center	BDKB200000
Human CHRM5 in pcDNA3.1+	Missouri S&T cDNA Resource Center	MAR0500000
Human EDNRA in pcDNA3.1+	Missouri S&T cDNA Resource Center	EDNRA00000
Human HRH1 in pcDNA3.1+	Missouri S&T cDNA Resource Center	HRH0100000
Human PTHR1 in pcDNA3.1+	Missouri S&T cDNA Resource Center	PTHR100000
Mouse Gpr68 in pcDNA3.1-	Novartis AG Internal Collection	N/A
Mouse Piezo1 in pcDNA3.1-	Novartis AG Internal Collection	N/A
Rat TrpV4 in pcDNA3.1-	Novartis AG Internal Collection	N/A
Software and Algorithms		
LabView	National Instruments	http://www.ni.com/en-us/shop/labview.html
ScreenWorks 3.1	Molecular Devices	https://www.moleculardevices.com/systems/flipr-tetra-high-throughput-cellular-screening-system#tab-2
Burrows-Wheeler Aligner	Li H. and Durbin R.	http://bio-bwa.sourceforge.net/
Nanozoomer	Hamamatsu	https://www.hamamatsu.com/jp/en/U12388-01.html
Other		
FLIPR	Molecular Devices	Tetra
Fura-2, AM	ThermoFisher	F14185
Fluo-3, AM	ThermoFisher	F1242
RBS lysis buffer	eBioscience	00-4333-57
Mouse Fc Block	BD Biosciences	553141
Trizol LS	ThermoFisher	10296028
Collagenase IV	ThermoFisher	17104019
Papain	Worthington	LS003119
RNeasy Mini Kit	QIAGEN	74106
Ovation RNA-Seq System V2	NuGEN	7102-A01
Ovation Ultralow Library System V2	NuGEN	0344NB-A01
High Sensitivity DNA Analysis Kit	Agilent Technonogies	5067-4626
Liberase	Millipore Sigma	5401020001
Lipofectamine 2000	ThermoFisher	11668027
Trypsin	Lonza	BE02-007E
6 μm-diameter fluorescent beads	ThermoFisher	A16504
BD BioCoat Laminin/Fibronectin Multiwell Plates	BD Biosciences	08-772-65

CONTACT FOR REAGENT AND RESOURCE SHARING

Further information and requests for resources and reagents should be directed to and will be fulfilled by the Lead Contact, Ardem Patapoutian (ardem@scripps.edu).

EXPERIMENTAL MODEL AND SUBJECT DETAILS

Animals

All procedures involving animal handling were approved by Institutional Animal Care and Use Committees (IACUC) of Genomics Institute of the Novartis Research Foundation (GNF), The Scripps Research Institute (TSRI) and CNRS Angers University. In addition, FMD and FMR experiments were performed in agreement with the guidelines from Directive 2010/63/EU of the European Parliament on the protection of animals used for scientific purposes.

Gpr68 knockout mice breeders ($Gpr68^{tm1.1Yaxu}$, C57BL/6J background, MGI ID: 3849457) were provided by Dr. Yan Xu (Indiana University School of Medicine). *Gpr68-eGFP* reporter mice (Tg(Gpr68-EGFP)IU33Gsat/Mmucd, RRID:MMRRC_031057-UCD) were purchased from GenSat Project from The Rockefeller University. All animals were in specific pathogen-free environment at GNF, TSRI and CNRS Angers University. They were housed in a 12 h light/dark cycle (light from 6 AM to 6 PM local time) in a temperature-controlled room (24°C) with free access to food and water. All mice were not involved in procedures and are drug and test naive. *Gpr68* knockout colony was maintained with Het x Het mating scheme and *Gpr68-eGFP* colony was maintained with het x WT scheme. 3 to 5 month- old male mice were used in the experiments with wild-type male littermates as controls as required.

Cell lines and cell culture

HEK293T cells were grown in Dulbecco's modified Eagle's medium containing 4.5 mg/ml glucose, 10% fetal bovine serum, 1 × antibiotics/antimycotics. The human cell lines used in screening for shear stress-sensitive ones are purchase from American Type Culture Collection (ATCC) and Japanese Collection of Research Bioresources (JCRB) Cell Bank as a part of National Cancer Institute 60 Cancer Cell Panel (NCI-60). The cell lines were maintained in ATCC recommended media and conditions. Detailed culture information could be found on https://www.atcc.org/ by searching for catalog numbers of the cell line (listed in the Key Resources Table). Cell line authentication information was supplied by ATCC. We were not able to obtain information on the sex of the cell line that are discontinued by vendors.

The mouse primary endothelial cells are isolated from male *Gpr68* KO and *Gpr68-eGFP* mice age 3-5 months. Cells were cultured in Endo-PM media (Navone et al., 2013) on laminin / fibronectin coated plates (BD Biosciences) at 37°C, 5% CO_2, with media changes every 2 days.

METHOD DETAILS

Constructs and Compounds

Human GPR68, GPR132, AGTR1, AVPR1A, BDKRB2, CHRM5, EDNRA, HRH1, PTHR1 were purchase from Missouri S&T cDNA Resource Center. Mouse Gpr68 in pCDNA3.1 was from Novartis internal collection. Expression constructs of human GPR68 and mouse Gpr68 were sub-cloned into pIRES2-EGFP vector by inserting the coding sequence (CDS) of genes at EcoRI and BamHI sites. The final CDS of human GPR68 in the constructs was the following:

ATGGGGAACATCACTGCAGACAACTCCTCGATGAGCTGTACCATCGACCATACCATCCACCAGACGCTGGCCCCGGTGGTCTA
TGTTACCGTGCTGGTGGTGGGCTTCCCGGCCAACTGCCTGTCCCTCTACTTCGGCTACCTGCAGATCAAGGCCCGGAACGAGCT
GGGCGTGTACCTGTGCAACCTGACGGTGGCCGACCTCTTCTACATCTGCTCGCTGCCCTTCTGGCTGCAGTACGTGCTGCAGCA
CGACAACTGGTCTCACGGCGACCTGTCCTGCCAGGTGTGCGGCATCCTCCTGTACGAGAACATCTACATCAGCGTGGGCTTCCT
CTGCTGCATCTCCGTGGACCGCTACCTGGCTGTGGCCCATCCCTTCCGCTTCCACCAGTTCCGGACCCTGAAGGCGGCCGTCG
GCGTCAGCGTGGTCATCTGGGCCAAGGAGCTGCTGACCAGCATCTACTTCCTGATGCACGAGGAGGTCATCGAGGACGAGAACC
AGCACCGCGTGTGCTTTGAGCACTACCCCATCCAGGCATGGCAGCGCGCCATCAACTACTACCGCTTCCTGGTGGGCTTCCTCT
TCCCCATCTGCCTGCTGCTGGCGTCCTACCAGGGCATCCTGCGCGCCGTGCGCCGGAGCCACGGCACCCAGAAGAGCCGCAA
GGACCAGATCCAGCGGCTGGTGCTCAGCACCGTGGTCATCTTCCTGGCCTGCTTCCTGCCCTACCACGTGTTGCTGCTGGTGCG
CAGCGTCTGGGAGGCCAGCTGCGACTTCGCCAAGGGCGTTTTCAACGCCTACCACTTCTCCCTCCTGCTCACCAGCTTCAACTG
CGTCGCCGACCCCGTGCTCTACTGCTTCGTCAGCGAGACCACCCACCGGGACCTGGCCCGCCTCCGCGGGGCCTGCCTGGCC
TTCCTCACCTGCTCCAGGACCGGCCGGGCCAGGGAGGCCTACCCGCTGGGTGCCCCCGAGGCCTCCGGGAAAAGCGGGGCC
CAGGGTGAGGAGCCCGAGCTGTTGACCAAGCTCCACCCGGCCTTCCAGACCCCTAACTCGCCAGGGTCGGGCGGGTTCCCCA
CGGGCAGGTTGGCCTAG

The final CDS of mouse Gpr68 in the constructs was the following:

ATGGGGAACATCACTACAGAAAACTCCTCACTATCTTGCCCCATCGACCACACCATCCACCAGACACTAGCCCCAGTGGTCTAT
GTGACCGTGCTGGTGGTGGGCTTCCCAGCCAACTGCCTGTCCCTCTACTTCGGGTACTTGCAGATCAAGGCCCGGAATGAGCTG
GGAGTGTACCTGTGTAACCTGACCATTGCAGACCTGTTCTATATCTGTTCACTTCCCTTCTGGCTGCAGTACGTGCTTCAGCACGA
CGACTGGTCCCATGGTGACCTATCCTGCCAGGTGTGTGGCATCCTCCTCTATGAGAACATTTACATCAGCGTGGGCTTCCTCTGC
TGCATCTCCATCGACCGCTACCTGGCTGTGGCCCACCCCTTCCGCTTCCACCAGTTCCGCACCCTGAAGGCAGCCGTGGGTGTC
AGTGTGCTCATCTGGGCCAAGGAGCTGCTGACCAGCATCTACTTCCTCAATCACAAGGAGGTCATTGAGGACGAGGACCAGCAC
CGAGTCTGCTTTGAGCATTACCCTATCCAGGCCTGGCAGCGTAGCATCAACTACTACCGCTTCCTGGTGGGCTTTCTCTTCCCCA
TCTGCCTGCTGCTGGCCTCCTACCAGGGCATCCTGCGGGCTGTGCGCCGCAGCCACGGCACACAGAAGAGCCGCAAGGACCA
GATTCAGCGGCTGGTGCTCAGCACCGTGGTCATCTTCCTGGCTTGCTTTCTACCCTACCACGTGCTGCTGCTGGTACGCAGCCT
CTGGGAGAGAAACTGTGAGTTTGCCAAGAGCATCTTCAACGTCTATCACTTCTCCCTCCTCCTCACCAGCTTCAACTGTGTAGCTG
ACCCGGTGCTGTACTGCTTTGTCAGTGAGACCACTCACAGGGACCTAGCCCGCCTCCGAGGAGCCTGCCTAGCTGTCCTTACCT
GCTCTAGGACAAGCAGGGCCAGGGAGGCCTACCCTCTGGGTGCCCCTGAGGCCTCTGGGAAAAGTGGGGCCCAGGGCGAGGA
ACCTGAATTGTTAACCAAGCTCCACTCAGCCTTCCAGACCCCTAGCTCACTGGGAGTGGGAGGGCCCTCCACAGTGGGGTTGG
CCTAG

Constructs of mouse Piezo1 and rat TrpV4 were described previously (Coste et al., 2010). Briefly, a 7.644 kb fragment of mouse Piezo1 CDS was amplified from cDNA libraries generated from Neuro2A total RNA using primers mPiezo1 fwd (5′ atggagccgca cgtgctg 3′) and mPiezo1 rev (5′ ctactccctctcacgtgtcca 3′) and cloned into pcDNA3.1(-) (Invitrogen) with NotI and HindIII restriction sites. A cDNA encoding TRPV4 was amplified from a rat kidney RNA library and cloned in pcDNA3.1 (-). All constructs were fully sequence verified. Agonists for the human GPCRs listed above and the PLC inhibitor U73122 were purchased from Tocris Bioscience. Ogerin (ZINC67740571) was synthesized by WuXi AppTek as a part of contract research services. The structure of Ogerin was described previously (Huang et al., 2015).

Engineering

Construction of the high-throughput shear stress stimulation system

The high-throughput disturbed flow system utilizes a 384-pin array printed by Projet MJP 3500 (3D Systems) using UV-cured Visijet Crystal resin (3D Systems). The circular face of the pin is 2.8mm in diameter. A square diaphragm neodymium subwoofer driver (W3-1750S, Tang Band) is used as the driver. A miniature 3-axis accelerometer (ADXL326, Analog Devices) affixed to array monitors the motion of the array. The assembly sits on a machined aluminum assay plate guide. Shims and set screws are employed to accurately align the array with the assay plate. A custom interface is written using LabView (National Instruments) which allows the user to set frequency, amplitude and duty cycle of the stimulation. The signal is sent to an amplifier (D-150A II, Crown) to drive the pin and create fluid motion. The accelerometer signal is acquired by a data acquisition card (USB-6341, National Instruments) and instantaneously displayed in LabView for the user to monitor the motion of the pin array.

Estimation of the shear stress intensity

The particle image velocimetery method used for estimating the shear stress intensity on the bottom of the assay well was described previously (Ranade et al., 2014). Briefly, we dispensed a suspension of 6 μm-diameter Texas Red fluorescent beads (Life Technologies) into the imaging chamber and let them settle to the bottom. We applied sine wave stimulations at 60Hz and imaged the motion of the beads at 500 frames per second using ORCA-Flash 4.0 CMOS camera (Hamamatsu). Images were analyzed using NIS-Elements (Nikon) and velocity values of ~60 beads were averaged for each input power setting. We calculated shear stress intensity at 3 μm above the surface of the coverslip as an approximation of that experienced by the cells cultured on the surface of the coverslip.

Cell-based Experiments

FLIPR assays

FLIPR experiments were performed as previous described (Ranade et al., 2014). Before loading, the cells were washed with assay buffer (1x HBSS with calcium and 10 mM HEPES, pH adjusted to 7.4) using ELx405 CW plate washer (BioTek). Cells were loaded with Fluo-3 for 60 min (4 μM Fluo-3, 0.04% F-127 in assay buffer) at 37°C. Cells were washed again with assay buffer and the plates were centrifuged at 15 g for 5 s before assayed on FLIPR Tetra (Molecular Devices). The data was analyzed on Screenworks 3.1 (Molecular Devices) by calculating the difference between the maximum and minimum fluorescence intensity during the course of recording, then normalize to the starting fluorescence intensity:

$$Fold\ of\ Response = (Fmax - Fmin)/Fstart$$

Disturbed shear stress stimulation

When applying shear stress with the high-throughput disturbed flow system, we first thoroughly dried the pin array with compressed air then mounted the 384-well plate on the system. Two stimulation protocols were used. The short protocol applies stimulation for 4 s at 60 Hz, and the long protocol applies 0.2 s pulses at 60 Hz every 2 s for 40 s. After each assay, the pin array was washed thoroughly with distilled water and air-dried before mounting onto the next plate. Whenever compounds were used, to avoid carry-over, the array was first thoroughly washed with 70% EtOH, then with distilled water and dried before assaying the next plate.

Laminar shear stress stimulation

HEK293T cells were plated in the Collagen IV-coated μ-slide I 0.4 laminar flow chambers (Ibidi) 24 h prior to experiments. After loading Fura-2, the chambers were mounted onto the microscope and connected to the Ibidi perfusion pump. Cells were given pulsatile (1 Hz) or continuous laminar flow for 120 s.

Plasmid DNA and siRNA transfection

For DNA plasmid transfection with HEK293T cells in poly-D-Lysine coated 384-well assay plates (Greiner Bio-One), we use 65ng plasmid, 0.195 μl Fugene 6 (Roche) and 1×10^4 cells in 40 μl standard growth medium for each well. When transfecting HEK293T cells on poly-D-Lysine glass coverslips (BD Biosciences), we use 500 ng of plasmids, 1.5 μl Fugene 6 and 1×10^5 cells in 600 μl growth medium. For laminar flow chamber experiments, cells were first transfected in 24-well plate in the same condition. 24h later they were trypsinized and plated in μ-slides I 0.4 flow chambers (Ibidi). Cells were assayed 48h post-transfection.

For siRNA transfection in 384-well plates, we mixed 1 pmol siRNA with 20 μl Opti-MEM and 0.15 μl Lipofectamine RNAiMax (Life Technologies)in each well, incubated for 20 min at room temperature, then added 20 μl cells (6×10^3 cells per well for MDA-MB-231, 1×10^4 cells per well for HeLa). When transfecting siRNA on glass coverslips, 20 pmol siRNA, 1 μl RNAiMax and 100 μl Opti-MEM were mixed and incubated for 20 min, then mixed with 500 μl cells (1×10^5 cells per well for HeLa, 2×10^5 cells per well for early passage HUVECs). SiRNAs were from Dhamacon. Cells were assayed 72h post-transfection.

Calcium imaging

Fura-2 single cell calcium imaging was performed as previous described (Ranade et al., 2014). Briefly, cells were seeded onto poly-D-Lysine coverslips (BD Biosciences). We loaded the cells with the ratiometric Ca^{2+} indicator Fura-2 AM (ThermoFisher) in imaging buffer (1x Hanks Balanced Salt Solution (HBSS) and 10 mM HEPES, pH adjusted to 7.4 by NaOH). After 30 minutes of loading at room temperature, coverslips were washed with imaging buffer and then mounted onto the disturbed shear stress imaging chamber and assayed at room temperature. The intracellular Ca^{2+} concentration was expressed as the 340/380 ratio.

High-throughput siRNA screen

To assemble a set of arrayed siRNAs targeting genes encoding multi-pass transmembrane (MPTM) proteins, we subjected 34,226 non-identical protein sequences extracted from the August 21, 2011 version of Human Refseq to sequence-based membrane topology and signal peptide prediction using the Phobius algorithm and website, identifying 2,907 human genes encoding one or more MPTM proteins (Käll et al., 2004, 2007). An unconstrained prediction model was employed, signal peptides annotated where predicted, and all two-pass or more predictions collapsed from protein to gene space to ensure that no siRNAs targeting non-MPTM protein isoforms were excluded. The siRNA library was picked from a genome-wide siRNA library and arrayed in 384-well poly-D-Lysine coated assay plate with one single oligo in each well (63 plates in total). MDA-MB-231 cells were transfected with the siRNA using a robotic liquid handler and incubated in a robot-assisted incubator (GNF Systems). Cells were assayed after 72h with HT disturbed shear stress system. Wells with calcium signal 3 × standard deviations below the plate mean were considered as hit wells. Genes with more than 3 hit wells were considered hits. We then crosschecked the bioinformatics results and the literature to filter out the hits that have known functions unrelated to acute (second-scale) calcium signaling. We picked the siRNA against hit genes from primary screen from the original genome-wide library and carried out a reconfirmation screen. For final screen, we purchased smartpool siRNA (Dharmacon OTP siRNAs, GE Healthcare) against the hits from the reconfirmation screen. For controls, in addition to PIEZO1 siRNA, we also included siRNA against a SERCA Ca^{2+}-ATPase (ATP2A2) to control for the effect of intracelluar calcium store.

Real-time pH measurement

2′,7′-Bis(3-carboxypropyl)-5(6)-carboxyfluorescein (BCEFC) was selected as pH indicator based on its dynamic range (pH6∼pH8), which fits GPR68 activation range best among all pH-sensitive dyes. BCECF increase fluorescence when pH increases. Free BCECF was used to monitor extracellular pH and its cell-permeable acetoxymethyl (AM) ester version was used for monitoring intracellular pH. Cells in assay plates were first washed with HBSS-pH7.4 on an ELx405 CW plate washer (BioTek). BCECF was then incubated with cells for 1 h at 37°C. When measuring intracellular pH, cells were then washed with HBSS-pH7.4 again. When measuring extracelluar pH, no wash step was added. Fluorescence was read on FLIPR for 10 s and acid or base were added to the buffer to shift pH to various final values from pH6.1 to pH8.3, while fluorescence was continuously monitoring for additional 150 s. For shear stress stimulation, fluorescence was recorded for 10 s and disturbed flow was applied for 60 s. Data was analyzed by ScreenWorks 3.0 (Molecular Devices) by exporting the real-time fluorescence values of the recordings corresponding to each treatment.

Fluorescence-activated Cell Sorting

Spleens from Gpr68 eGFP reporter mice were isolated and dissociated in FACS buffer (PBS containing 2% FBS and 2 mM EDTA) and red blood cells were lysed using RBC Lysis Buffer (eBioscience). Samples were washed once in FACS buffer, filtered through 100 μm diameter nylon mesh, and incubated with FcBlock (BD Biosciences) for 5 minutes at room temperature. They were then stained with BV421 CD4 (Biolegend), BV650 CD3 (Biolegend), APC-Cy7 CD19 (Biolegend), PerCP-Cy5.5 CD8 (BD Biosciences), and APC NK1.1 (eBioscience) for 20 min at 4°C in the dark. The cells were washed once then resuspended in FACS buffer. Data was acquired using a LSRII flow cytometer (BD Biosciences) and was analyzed using Flowjo (Treestar). Populations were defined as follows: CD4T cells: $CD3^+$ $CD4^+$ $CD8^-$, CD8T cells: $CD3^+$ $CD8^+$ $CD4^-$, B cells: $CD3^-$ $NK1.1^-$ $CD19^+$, NK cells: $CD3^-$ $NK1.1^+$ $CD19^-$. For cell sorting, spleens were processed and stained as above, but were sorted using a FACSAria II Cell sorter (BD Biosciences) into Trizol LS (ThermoFisher) and processed as previously described.

RNA sequencing of mouse bladder MVECs

The Gpr68 eGFP reporter mice were sacrificed with CO2 and the bladders were dissected out and cut into small pieces with micro scissors in PBS. The tissues were digested with 12.5 mg/mL collagenase IV (ThermoFisher) and 10 U/mL papain (Worthington) at 37°C for 1 h. The suspension was triturated with fire-polished glass pipettes and then spun down to collect the cell pellet. After washing the pellet twice with PBS, the cells were suspended in FACS buffer. The cells were stained with CD31-APC and CD45-APC-Cy7 (BD Biosciences) for 20 min at 4°C in the dark, and stained with PI before sorting. We sorted the cells that are $CD31^+$ $CD45^-$ GFP^+ and $CD31^+$ $CD45^-$ GFP^- into two 1.5 mL tubes each containing 1ml Trizol LS (ThermoFisher). Total RNA was extracted and column purified using RNeasy kit (QIAGEN). For each condition, 2 ng of total RNA was used to produce Illumina-compatible sequencing libraries with Ovation Ultralow Library System V2 (NuGEN). The cDNA was then fragmented to ~200bp size range and prepared for RNA Sequencing by Ovation Ultralow DR Multiplex System (NuGEN) and the quality validated using High Sensitivity DNA Kit (Agilent Technologies). cDNA libraries were run on a HiSeq 1000 (Illumina) with 50 bp single-end reads. Reads were de-multiplexed with the Illumina pipeline. Raw reads were aligned to a reference FASTA file which contains a curated list of mouse transcripts, plus mitochondrial sequence, and mitochondrial transcripts, and Illumina adaptor sequences. Alignment was done with BWA (Burrows-Wheeler Aligner) (Li and Durbin, 2009) and RPKM values were created from the SAM output file (Li et al., 2009a). All samples contained at least 20 million mapped reads. Messenger RNAs less than 200 bp were eliminated from analysis.

Culturing of mouse primary cerebral MVECs

Whole cerebrum from Gpr68-eGFP reporter mice were isolated in cold PBS and homogenized in buffer containing 1x HBSS, 15mM HEPES and 1% dextran sulfate on ice. Equal volumes of 26% dextran sulfate was mixed well with the homogenized samples and centrifuged at 5800 g at 4°C for 10 min. The pellet was resuspended in 0.625mg/mL Liberase enzyme mix (Millipore Sigma) and digested at 37°C for 1hr (triturate once every 30 min using fire-polished glass pipette). Digestion was then stopped with cold isolation buffer and spun down. The pellet was resuspended in 25% BSA and spun for 15 minutes at 1500rpm at room temperature. The final pellet was resuspended in Endo-PM media (Navone et al., 2013) and plated onto laminin / fibronectin coated culture plates. Cells were cultured for at 37°C, 5% CO_2 until confluent with media changes every 2 days.

Lentiviral shRNA knockdown and laminar flow stimulation of MVECs

Dharmacon TRC shRNA constructs for murine Gpr68 were purchased from GE Healthcare. Gpr68 shRNA constructs were co-transfected with first generation packaging vectors using Lipofectamine 2000 (Life Technologies) according to the manufacturer's instructions into HEK293T cells. Medium was changed after 24hrs and the supernatant was collected 48hrs after transfection. We centrifuged the supernatant at 500 g for 10 min and added over cultured primary endothelial cells (400 μL of supernatant per well on 24-well plate). 24hrs after infection medium was replaced with Endo-PM containing 2 μg/mL puromycin. 48h post infection, the MVECs were gently dissociated using Trypsin (Lonza) and plated in μ-slide I 0.2 laminar flow chamber (Ibidi) and kept in Endo-PM with 2 μg/mL puromycin. 72 h later, cells were loaded with Fura-2 and calcium imaging experiments were conducted with pulsatile laminar flow (1Hz) stimulation.

In Vivo Experiments

Mesenteric arteries cannulation

1^{st}, 2^{nd} and 3^{rd} arterial segments were isolated from the mesenteric circulation and cannulated at both ends on glass micro-cannulae and mounted in a video-monitored perfusion system (Living System, LSI, Burlington, VT). Arterial segments were bathed in a 5 mL organ bath containing a physiological salt solution (PSS) of the following composition (in mM): 135.0, NaCl, 15.0, $NaHCO_3$, 4.6 KCl, 1.5, $CaCl_2$, 1.2, $MgSO_4$, 11.0, glucose, 10.0, N-2-hydroxyethylpiperazine-N-2-ethylsulfonic acid. The PSS was maintained at pH7.4, PO_2 160 mmHg, PCO_2 37 mmHg. Perfusion of arterial segments was obtained with 2 peristaltic pumps, one controlling flow rate and one under the control of a pressure-servo control system. Pressure at both ends of the arterial segment was monitored using pressure transducers. Arterial contractility was assessed with KCl (80 mM) and phenylephrine 1 μmol/L. Endothelium integrity was assessed with acetylcholine (1 μM) after precontraction with phenylephrine (50% of maximum contraction). Pressure was then set at 75mmHg and flow was increased by step (3 to 50 μl per min) through the distal pipette with a peristaltic pump. Arteries were then bathed in a Ca^{2+}-free PSS containing ethylene-bis-(oxyethylenenitrolo) tetra-acetic acid (2 mmol/L) and sodium nitroprusside (10 μmol/L). Pressure was then increased by step from 10 to 125 mmHg, in the absence of flow, in order to determine passive arterial diameter (Henrion et al., 1997).

Flow-mediated outward remodeling of resistance arteries

4-5-month old GPR68 KO and WT mice were submitted to surgery in order to increase blood flow in mesenteric artery as previously described (Caillon et al., 2016). Briefly, 3 consecutive first-order mesenteric arteries were used. Ligatures were applied to second-order branches as shown on Figure 7C. The artery located between the two ligated arteries was designed as high flow (HF) artery. Arteries located at distance of the ligated arteries were used as control (normal flow, NF). In this protocol, animals were anesthetized with isoflurane (2.5%). They were treated with buprenorphine (Temgesic; 0.1 mg/kg, s.c.) before and after surgery.

Mice were sacrificed after 14 days before collection of HF and NF first order arteries and of the corresponding HF and NF third order mesenteric arteries. Their passive diameter was then measured using pressure arteriography as describe above.

Blood pressure radiotelemetry

Pressure radio transmitters (HD-X11, Data Science International) were implanted into left carotid artery according to Manufacturer's recommended procedure. Blood pressure and heart rate were recorded continuously and exported as 5-minute segments. Baseline

blood pressure and heart rate data was averaged from last day of baseline measurements of all cohorts (usually 3rd or 4th day after the start of recording to obtain consistently stable measurements).

Ultrasound echocardiography

Mice were continuously anesthetized by isoflurane at a concentration of 3-4% (induction) and 1-2% (maintenance) mixed with 1 L/min 100% O_2 and immobilized on a heating platform to maintain the body temperature at 37°C ± 0.5°C. Heart rate (HR) and respiratory physiology were continuously monitored by ECG electrodes. They were analyzed by B-mode and M-mode echocardiography using Vevo3100 ultrasound imaging system with a MX550D 40 MHz linear array transducer (VisualSonics). All M-mode measurements were performed with Vevo LAB v.3.1.0 in end-diastole and end-systole. End-diastolic and end-systolic measurements were obtained at the time of maximal internal chamber dimensions and at the minimal internal chamber dimensions, respectively. The LV structural parameters measured from short axis view in M-mode were used in the calculation of LV ejection fraction (EF) and LV fractional shortening (FS).

Miscellaneous

Quantitative reverse transcriptase PCR

For tissue qPCR, DRG were freshly isolated from adult C57BL/6J wild-type mice and snap frozen on dry ice and total RNA was isolated using Trizol/choloform method. Total RNA from all other tissues was purchased from Zyagen. For qPCR using cultured cells, samples were lysed with Trizol and total RNA was isolated using chloroform/isopropanol precipitation. 100-200ng of total RNA was used to generate cDNA using the Quantitect Reverse transcript kit (QIAGEN). Real time Taqman PCR assays for mouse and human Gpr68 were purchased from Life Technologies (assay id: Mm 00558545_s1 and Hs 00268858_s1) and IDT (Mm.PT.58.42531755 and Hs.PT.58.27651490.g) with a FAM reporter dye and a non-fluorescent quencher.

We used FastStart Universal probe master mix (Rox) (Roche). The reaction was run in the 7900HT fast real time system (ABI) using 0.5ul of the cDNA in a 10ul reaction according to the manufacturer's instructions in triplicate. Calibrations and normalizations were done using the$2^{-\Delta\Delta CT}$ method (Livak and Schmittgen, 2001), where ΔΔCT = ((CT (target gene) -CT (reference gene)) - (CT (calibrator) - CT (reference gene). Gapdh and b-actin were used as the reference genes.

Immunostaining

For GFP immunostaining experiments, tissues from various organs were collected from 7-week-old wild-type and Gpr68 eGFP reporter mice after perfusion with 4% PFA. Tissues were briefly fixed in 4% PFA and were dehydrated through an ethanol series/xylene and embedded in paraffin. 5μm sections were cut and incubated with blocking solution containing 1x PBS, 10% blocking serum, 3% BSA and 0.4% Triton X-100 for 1hr at room temperature. Slides were stained overnight with a goat anti-GFP antibody (Lifespan Biosciences). Slides were treated with Omni-Map anti -goat secondary antibody conjugated with HRP (Ventana) followed by development using the Chromo Map DAB kit (Ventana). Slides were mounted with Cytoseal and scanned using the Nanozoomer 2.0 HT (Hamamatsu).

We tested murine Gpr68 antibodies from Lifespan Biosciences (LS-A3968 and LS-A1194) and antibodies custom generated at Pierce Biotechnologies (peptide sequences: RTSRAREAYPLGAPEASGK and EEPELLTKLHSAFQTPSSLG). We determined that none of the above can specifically detect Gpr68 protein in HEK293T cells overexpressing murine Gpr68 in our immunohistochemistry experiments.

In situ hybridization

Tissues from C57BL/6J mice were isolated after perfusion and fixed in 10% formalin overnight. The tissues were dehydrated through an ethanol series/xylene and embedded in paraffin. 10μm sections were cut and *in situ* hybridization was carried out using the RNAscope assay (ACD Bio). Development of signal was done using the RNAscope 2.0 HD brown detection kit. Probes for mGpr68 (cat. #: 319321) and DapB negative control (cat #: 310043) were purchased from Advanced Cell Diagnostics. Slides were mounted with Cytoseal and scanned using the Nanozoomer 2.0 HT (Hamamatsu).

QUANTIFICATION AND STATISTICAL ANALYSIS

Unless otherwise noted in Results and figure legends, statistical significance was evaluated using unpaired two-tailed Students's t test when comparing the difference between two samples, and one-way ANOVA was employed when comparing the samples among groups with more than two samples. All data plotted as mean ± SEM. For experiments that includes samples taken from animals, n represent the number of animals used in the analysis.

DATA AND SOFTWARE AVAILABILITY

RNaseq data of Gpr68-eGFP endothelial cells discussed in this publication have been deposited in NCBI's Gene Expression Omnibus and are accessible through GEO Series accession number GEO: GSE111784 (https://www.ncbi.nlm.nih.gov/geo/query/acc.cgi?acc=GSE111784)

Cell

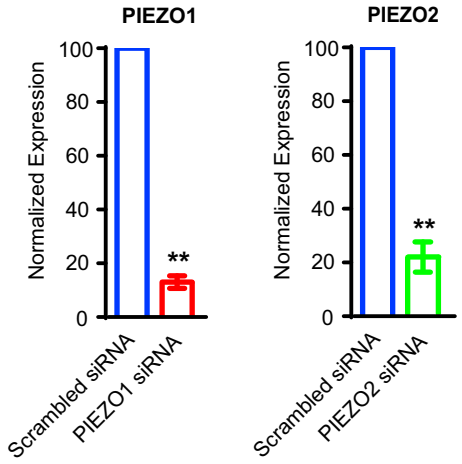

Figure S1. Transfecting MDA-MB-231 with PIEZO1 or PIEZO2 siRNA Significantly Knocks Down Their Respective mRNA Levels, Related to Figure 1

Relative mRNA level of PIEZO1 and PIEZO2 in MDA-MB-231 cells transfected with PIEZO1 siRNA or PIEZO2 siRNA compared with cells transfected with scrambled siRNA (mean ± SEM from 4 trials).

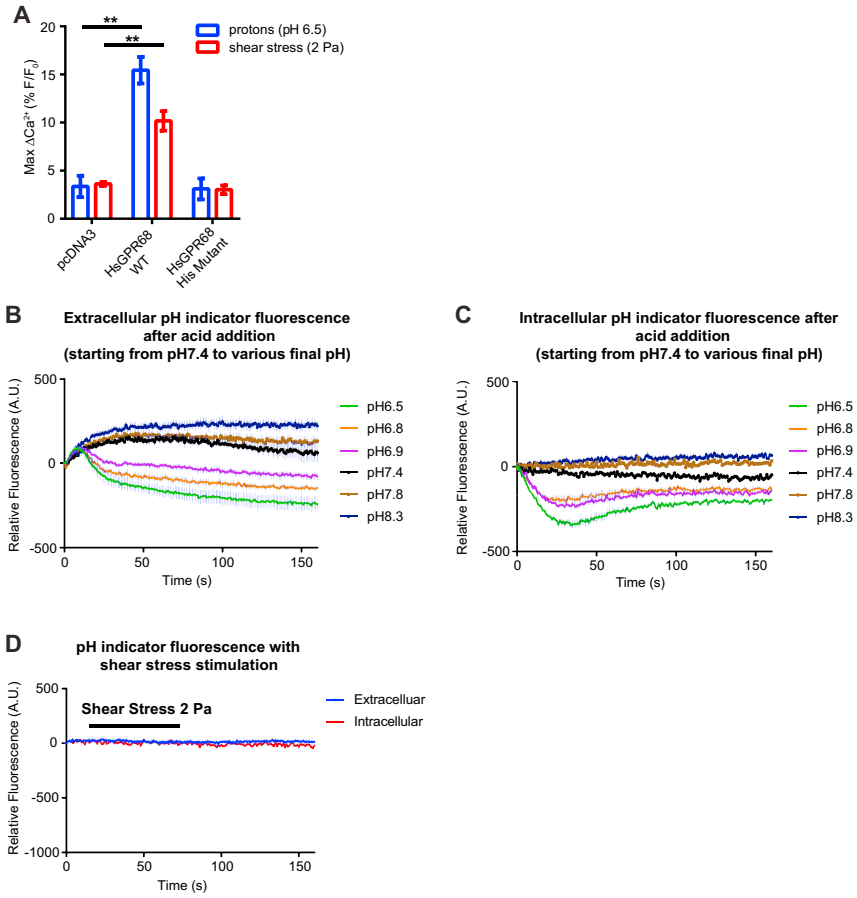

Figure S2. Characterization of GPR68 Activation Mechanisms, Related to Figure 3

(A) HEK293T cells were transiently transfected with pcDNA5, GPR68 WT or GPR68 histidine mutant constructs. Acid or shear stress-induced calcium transients were assayed 48h after transfection. For acid stimulation, the final pH was pH6.5. For shear stress stimulation, a 4 s pulse of 60 Hz disturbed flow at 2 Pa was applied to the cells. Results were plotted as mean ± SEM from 3 trials.

(B and C) assessment of pH-sensitive fluorescent dye BCECF for measurement of extracellular and intracellular pH. Upon addition of acid or base to cells to shift the buffer pH to various final pH (from pH6.5 to pH8.3), BCECF fluorescence intensity changed accordingly, demonstrating that the dye is sensitive to distinguish minute changes in pH.

(D) Upon application of shear stress, there's no measurable change in BCECF fluorescence, indicating no changes in either extracellular or intracellular pH. Traces are plotted as mean ± SEM from two trials, 16 repeats for each condition.

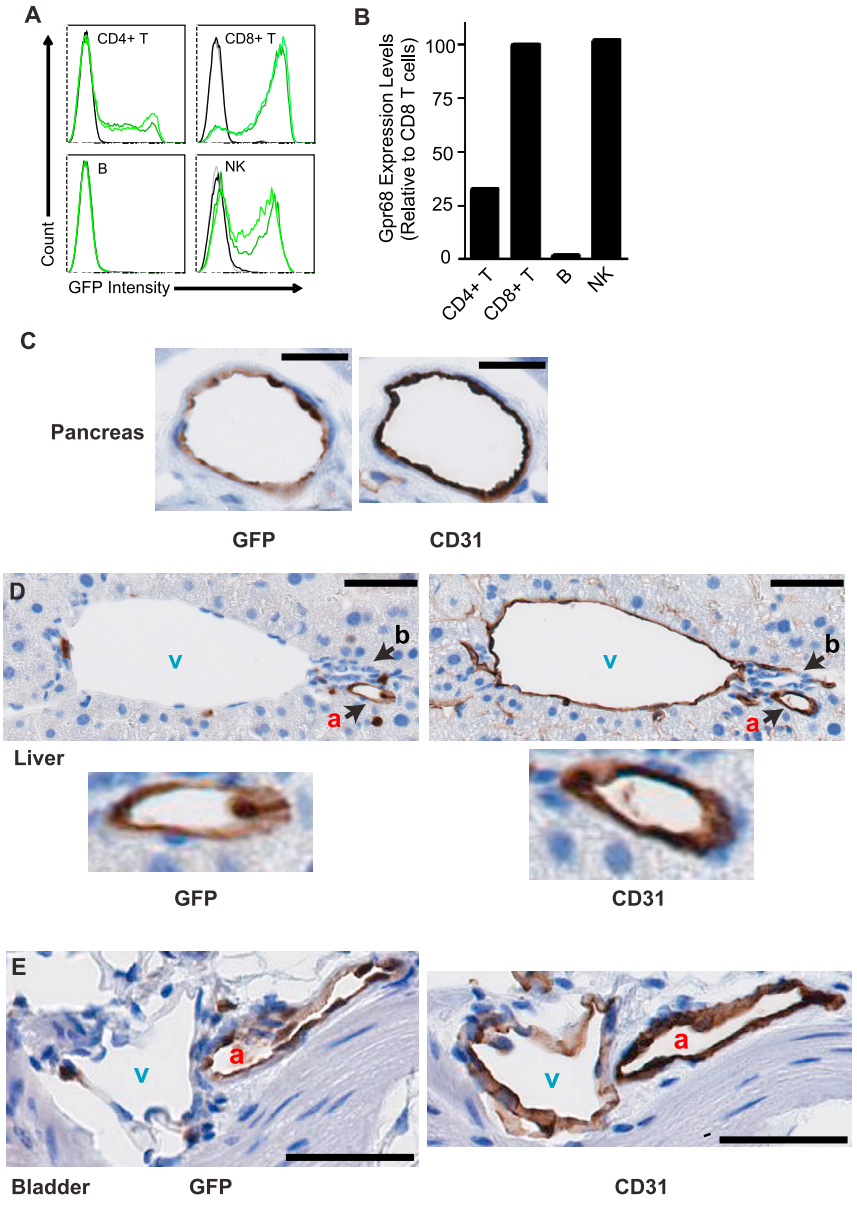

Figure S3. GFP Immunoreactivity Is Detected in Small-Diameter Arteries in Various Tissues of GPR68-eGFP Reporter Mice, Related to Figure 5

(A) Flow cytometry analysis of GFP intensity in various populations of leukocytes isolated from the spleen of Gpr68 eGFP reporter mice. Results were from two eGFP reporter mice (light and dark green lines) and two C57B/L6 mice (gray and black lines).

(B) Relative mRNA level of Gpr68 in various populations of leukocytes isolated from the spleen of C57B/L6 mice.

(C) Representative images of antibody staining against GFP and CD31 in blood vessel of pancreas isolated from Gpr68 eGFP reporter mice. Scale bar: 25 μm.

(D) Representative images of antibody staining against GFP and CD31 in blood vessel of liver. **a**, artery; **b**, bile duct; **v**, portal vein. Scale bar: 25 μm.

(E) Representative images of antibody staining against GFP and CD31 in blood vessel of bladder. **a**, artery; **v**, vein. Scale bar: 50 μm. tissues from 4 mice were examined.

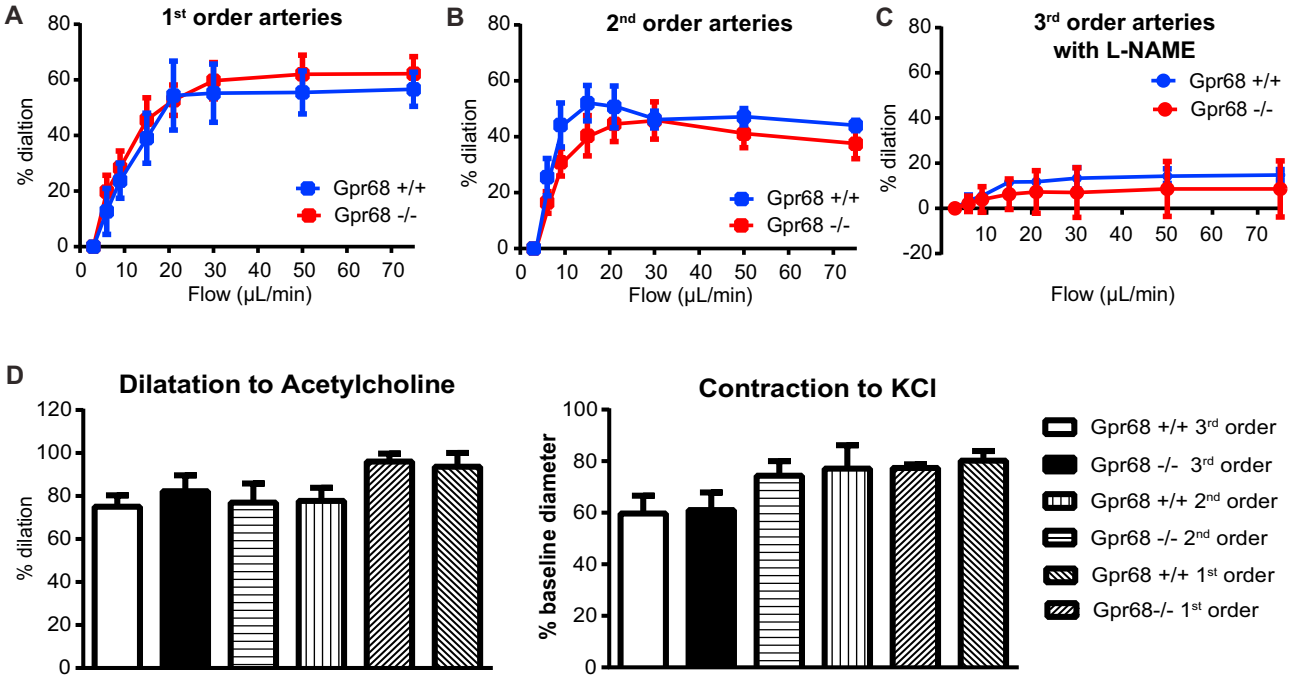

Figure S4. Gpr68 KO First- and Second-Order Mesenteric Vessels Have Normal Response to Flow and Vessels of All Sizes Have Normal Response to Chemical Stimulations, Related to Figure 7

(A and B) FMD in first and second order MAs from Gpr68 KO mice and WT littermates. n = 7 Gpr68 KO and n = 7 WT for 2nd order arteries, and n = 4 Gpr68 KO and n = 5 WT for 1st order arteries.

(C) FMD response in 3rd order MAs in the presence of 100 µM L-N^G-Nitroarginine methyl ester (L-NAME). Vessels from 6 KO and 6 WT mice were tested.

(D) Dilation response of various orders of MAs to 1 µM acetylcholine and 80 mM of KCl. For acetylcholine experiment, 3rd order MAs, n = 5 for WT and n = 8 for KO. 2nd order MAs, n = 8 for WT and n = 7 for KO. 1st order MAs, n = 5 for WT and n = 5 for KO. For KCl experiment, 3rd order MAs, n = 8 for WT and n = 11 for KO. 2nd order MAs, n = 8 for WT and n = 10 for KO. 1st order MAs, n = 5 for WT and n = 5 for KO.

All results were plotted as mean ± SEM.

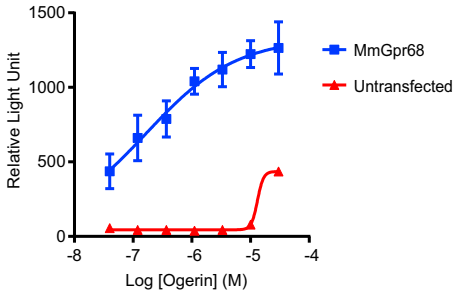

Figure S5. Ogerin Is a Mouse Gpr68 Agonist, Related to Figure 7

HEK293T cells were transiently transfected with mouse Gpr68. Relative fluorescence from calcium indicators were acquired for 10 s, then ogerin was added to the cells in various concentrations, while measurement continued for 180 s at 1 data point per second. Maximum fluorescence was plotted as mean ± SEM from 3 trials. Dose response curve fitting yielded an EC_{50} of 0.17 μM.

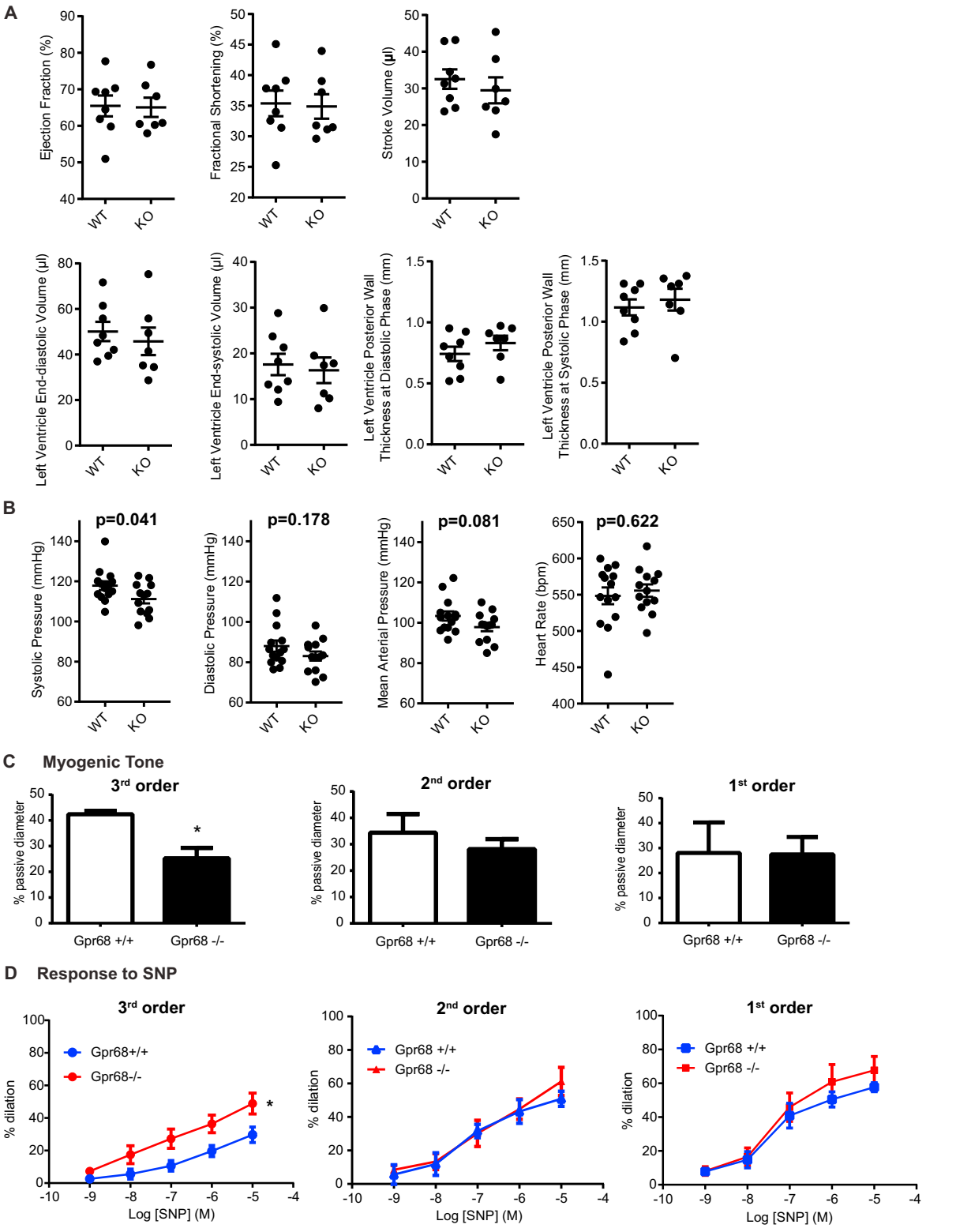

Figure S6. Characterization of Hemodynamic and Cardiac Parameters and Assessment of Mesenteric Vessels of Gpr68 KO Mice, Related to Figure 7

(A) Echocardiography assessment of Gpr68 KO and WT heart. All the structural parameters were not significantly different between KO and WT mice.

(B) Blood pressure radio telemetry recording of baseline hemodynamic parameters of Gpr68 KO mice and WT littermates. Each dot represents one animal.

(legend continued on next page)

(C) Myogenic tone of MAs from various orders. 3rd order MAs, n = 8 for WT and n = 10 for KO. 2nd order MAs, n = 7 for WT and n = 7 for KO. 1st order MAs, n = 3 for WT and n = 5 for KO.
(D) Dilation response of MAs to SNP at various dosages. For 3rd order MAs, 5 WT and 7 KO vessels were examined. 2nd order MAs, n = 4 for WT and n = 6 for KO. 1st order MAs, n = 4 for WT and n = 5 for KO.
All results were plotted as mean ± SEM.

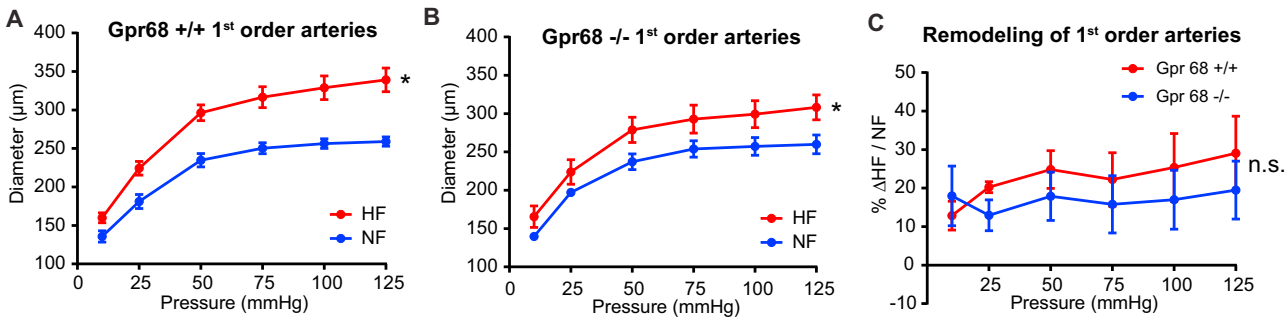

Figure S7. Assessment of Flow-Mediated Outward Remodeling of Gpr68 KO Mesenteric Vessels, Related to Figure 7

(A and B) Passive diameter distension curve at increasing pressures for WT and KO 1st order mesenteric arteries exposed to HF or NF. Both showed significant diameter increase in response to chronic HF (WT: $p = 0.017$ and KO: $p = 0.0315$).

(C) The extent of remodeling of 1st order mesenteric vessels from WT and KO are similar. All results are plotted as mean ± SEM.*$p < 0.05$, two way ANOVA for repeated-measures, n = 5 for Gpr68 KO and n = 6 for WT littermates. n.s., not significant.